MAGIC-TDAS 06-03
060308/DTescaro

Analysis of the observations of the AGN HB89-1553 during May 2005

D. Tescaro, A. Moralejo (IFAE)

March 8$^{\text{th}}$, 2006

Abstract

HB89-1553+113 (in the following HB-1553) is a rather distant (z>0.3 [1]) AGN of the BL Lac type. This source was observed by MAGIC during April and May 2005. An analysis performed by the Wüerzburg group, presented in the October 2005 collaboration meeting, showed some hint of a signal. An independent analysis of the May data is presented here. Some modest excess of gamma-like events is visible, although it does not seem convincing enough as to confidently claim a detection.

Contents

1 Introduction

The observation of HB-1553 was proposed by M. Hayashida, R. Wagner and D. Kranich for the first cycle of MAGIC observations. The request was based on the SSC flux prediction by Costamante and Ghisellini [2], which made this source one of the best AGN candidates, along with BL Lac. The detection of HB-1553 by MAGIC would be a most relevant result. Thanks to its large redshift, it could allow us to put strong constraints on models of the EBL.

An automatic analysis of several observed AGNs performed in Würzburg [3] resulted in a weak signal from this source. At MPI Munich the same data were analyzed by M. Hayashida using the standard Mars code, with encouraging results. The Berlin group, using mostly an independent analysis code, has also reported a signal on the same dataset. We have independently analyzed the HB-1553 data from May 2005, applying the same kind of analysis that has been used for the MAGIC observations published (or accepted for publication) until now. This method makes use of the *Random Forest* for background discrimination. Observations of Mrk 501 from the end of May have been analyzed in the same way and used to optimize the background supression cuts.

2 Data sample

The source has been observed during April (about 1.6h) and May 2005 (about 7.2h). The detector conditions during this period were not good due to several problems. Period 29 is the worst period concerning the pulse position problem, as can be seen from the studies of P. Liebing (see fig. 1) [5]. This makes signal reconstruction harder (since pulses may be partially outside of the FADC range). One has to deal also with all the difficulties related to the instability of the detector in different days (the pulse position depends for instance on the temperature of the electronics). A further discussion about this problem will be found in §4. Furthermore, between April and May the mirrors were refocused. After a refocusing the pointing model has to be rebuilt and some mispointing is to be expected before this is done. The average mispointing has been monitored by the Würzburg group [4]. The May data is split in two sub–periods corresponding to the beginning and the end of the month: we have a value of $0.069 \pm 0.038°$ (24) for the former and $0.031 \pm 0.028°$ for the latter[1]. Within the uncertainties, the values are close to those of April and June ($0.059°$ and $0.067°$ respectively).

[1] As reported by the authors of these estimates, the actual mispointing for the analyzed data can be bigger, being all low zenith angle observations.

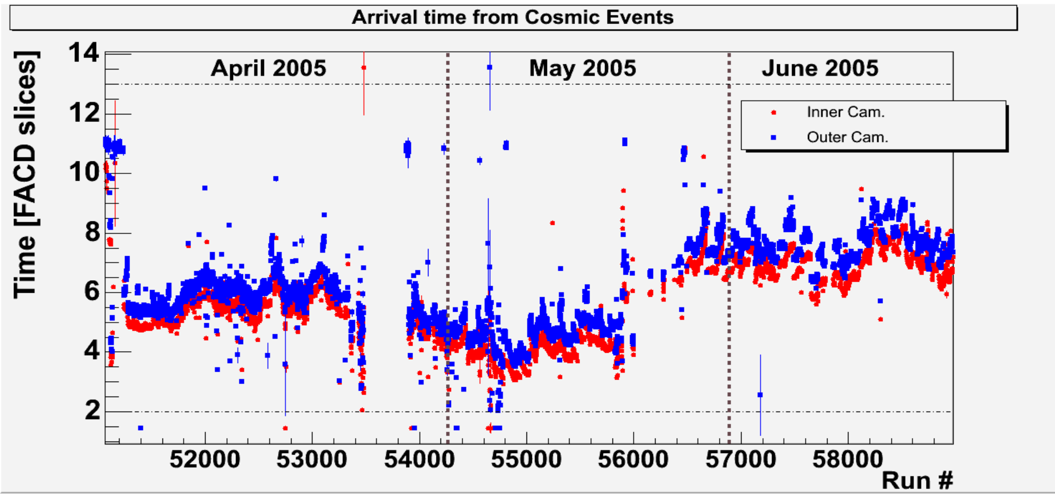

Figure 1: Mean arrival time in the FADC of pulses from air showers.

SOURCE	DAY (May 2005)	OBS.TIME (min)	ZA (deg)
HB–1553	03	103	18-23
HB–1553	09	57	18-24
HB–1553	10	133	18-25
HB–1553	10	95	18-28

Table 1: ON initial data sample.

SOURCE	DAY (May 2005)	OBS.TIME (min)	ZA (deg)
Off1ES1426-1	04	30	17-21
OffM87-1	06	76	17-27
OffHB1553-1	07	129	18-23
Off1ES1426-1	11	113	14-25
OffMrk501-1	30	50	17-27

Table 2: OFF initial data sample.

In the present work only the May data have been analyzed. A separate analysis would be needed for the April data set (due to the worse optical PSF before the mirror adjustment). Table 1 illustrates the starting ON data sample, for a total of 6.47 h of observation. 2.1 hours of specific OFF data have been taken for this source during the night[2] of May 7$^{\mathrm{th}}$, but much more OFF is available in the same period, with more or less the same Zenith Angle (ZA), for a total amount of about 6.63 hours (see table 2).

[2]The quoted dates are those after midnight, i.e., May 7$^{\mathrm{th}}$ refers to the night from 6$^{\mathrm{th}}$ to 7$^{\mathrm{th}}$.

3 Data processing and checks

The raw data have been processed directly in the Würzburg Data Center using the *condor* system provided. We used the *Mars_V0-11-5* program release (Barcelona version), and the *ROOT_v3.10.02* framework. The *callisto* and *star* executables have been run over the raw data listed above. The *callisto* settings are the default ones except for the extractor: we used MExtractTimeAndChargeSpline. This choice was motivated by the already mentioned fact that in the period considered the pulses come too early in the digitalization window. In those particular conditions the Spline extractor results more efficient than the Digital Filter (default) one. A further discussion can be found in §4. The cleaning method selected for the star hillas parameters computing is the so-called "Absolute", with levels of 7 and 5 photoelectrons for *core* and *boundary* pixels respectively.

3.1 ON data

Using the *star* files obtained, some quality data checks have been performed. First of all, the mean values (average over one run) of some interesting parameters (rate, SIZE, WIDTH, ZA, DIST and LENGTH) have been plotted as function of the run number. Figure 2 illustrates the global results while in figs. 3 to 6 the single day plots are shown. We notice that (except for May 10^{th}) the ON samples rates are around 270 Hz, and quite stable in time. May 10^{th} has a slightly lower rate and a clear drop starting from Run 55294. Runs from 55295 to 55304 have been excluded from the subsequent analysis for this reason. The most likely reason for this change in rate is the arrival of some clouds. On the runbook of this day the operators reported that some high clouds arrived just before stop the data acquisition of HB-1553.

3.2 OFF data

The same procedure has been applied to the OFF sample initially considered. The results are shown in figs. 7 (global plot) to 12. May4^{th} (first day of Off1ES1426) has been excluded from the OFF sample due to the low rate (190Hz) with respect to the ON and the other OFF samples. The OffHB1553, which represents the official OFF of the source, shows a relatively low rate (230 Hz), but looks otherwise normal, so we decided to consider it as good OFF. The average Hillas parameters seem stable, the same as for the ON sample.

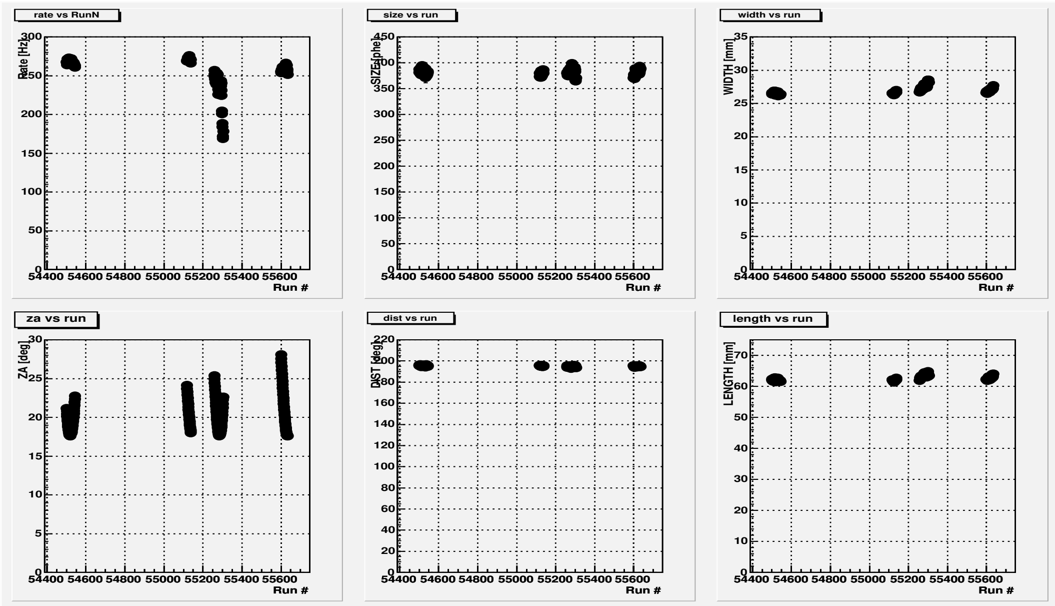

Figure 2: Whole ON sample (6.47 h). Plots of RATE, SIZE, WIDTH, ZA, DIST and LENGTH mean run values. No SIZE cut.

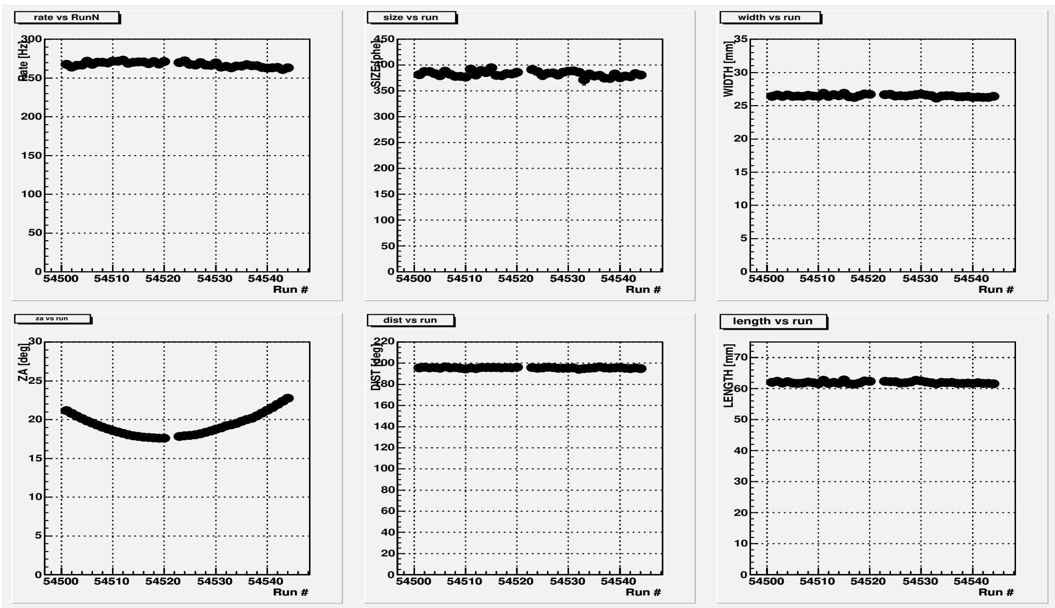

Figure 3: ON sample, May 3th (1.75 h). Plots of RATE, SIZE, WIDTH, ZA, DIST and LENGTH mean run values. No SIZE cut.

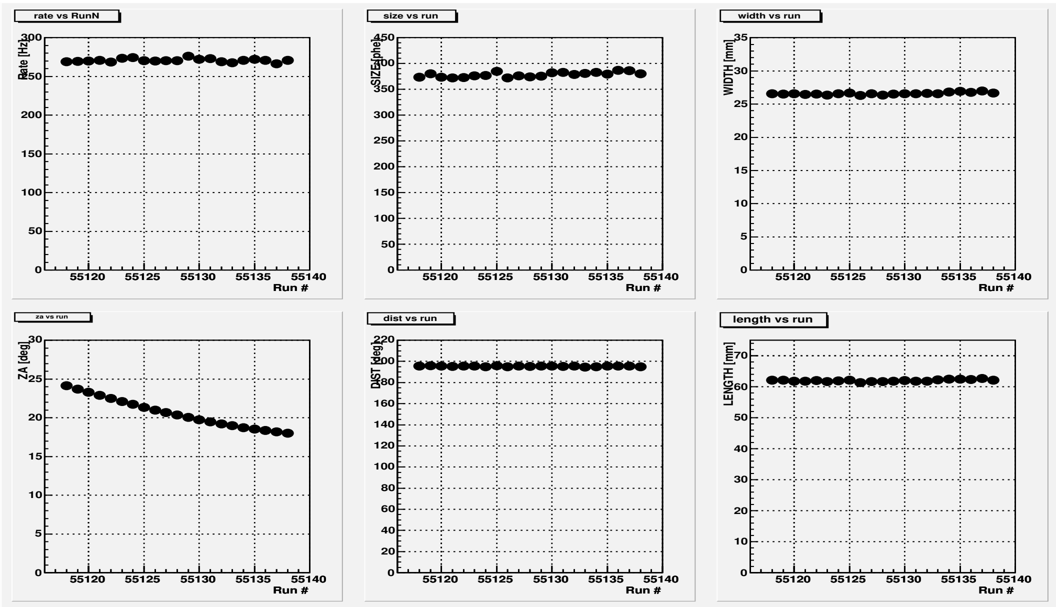

Figure 4: ON sample, May 9th (1 h). Plots of RATE, SIZE, WIDTH, ZA, DIST and LENGTH mean run values. No SIZE cut.

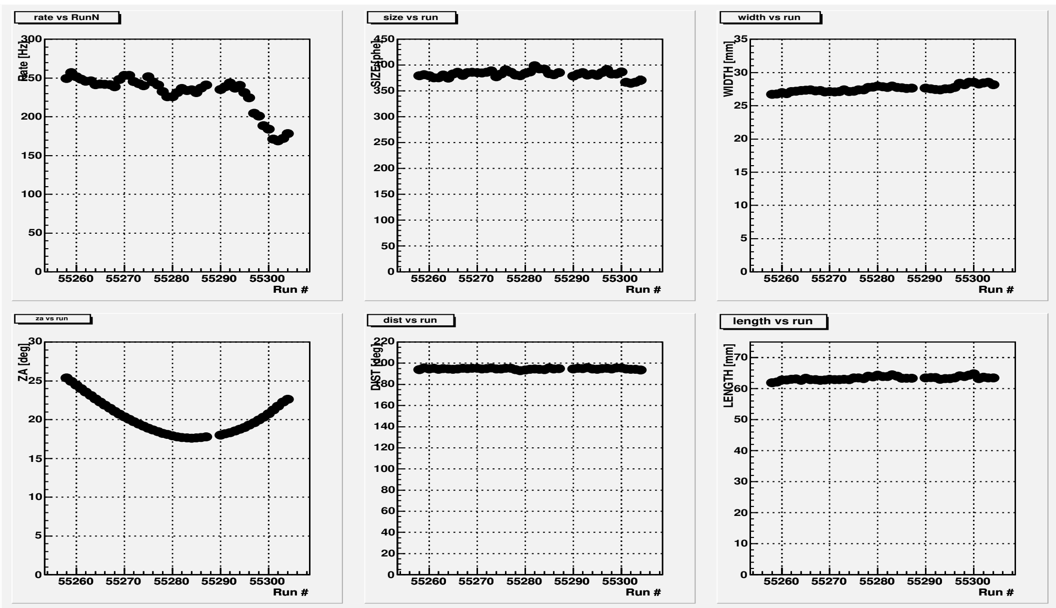

Figure 5: ON sample, May 10th (2.25 h). Plots of RATE, SIZE, WIDTH, ZA, DIST and LENGTH mean run values. No SIZE cut.

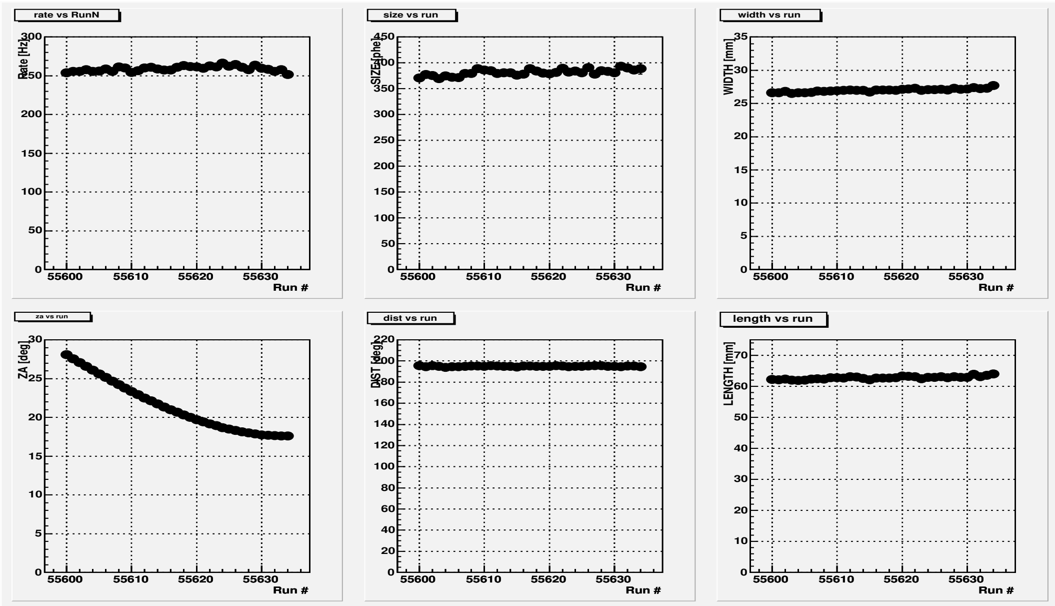

Figure 6: ON sample, May 13$^{\text{th}}$ (1.5 h). Plots of RATE, SIZE, WIDTH, ZA, DIST and LENGTH mean run values. No SIZE cut.

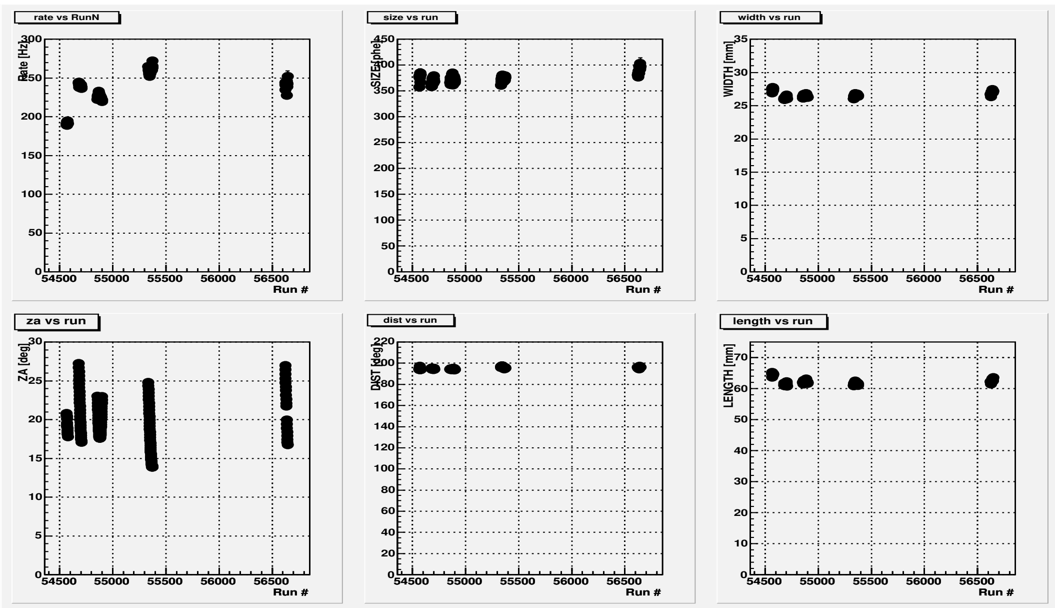

Figure 7: Whole OFF sample (6.63 h). Plots of RATE, SIZE, WIDTH, ZA, DIST and LENGTH mean run values. No SIZE cut.

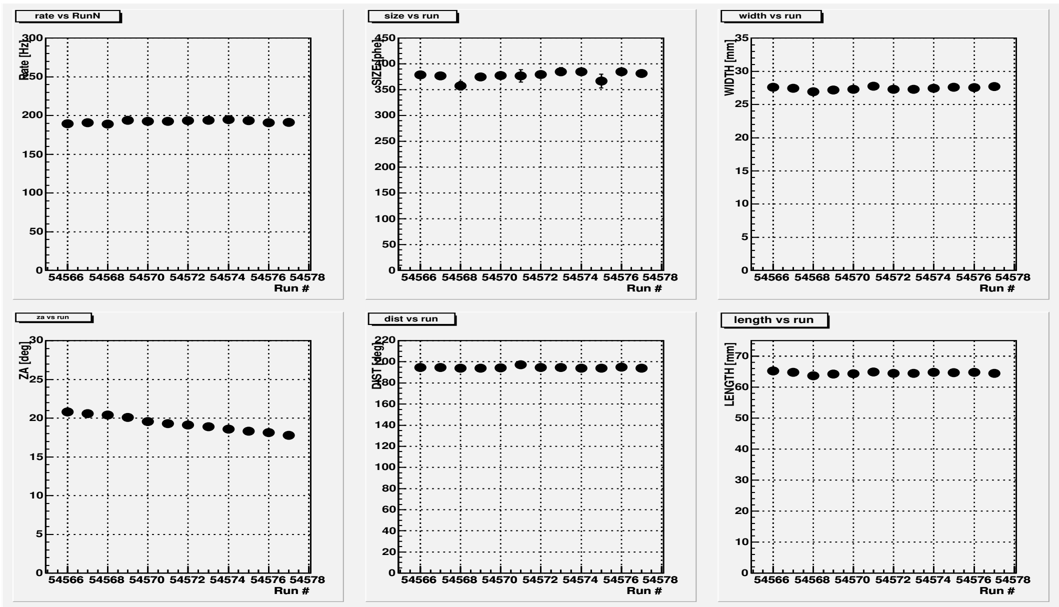

Figure 8: OFF sample (Off1ES1426), day May 4th (0.5 h). Plots of RATE, SIZE, WIDTH, ZA, DIST and LENGTH mean values. No SIZE cut.

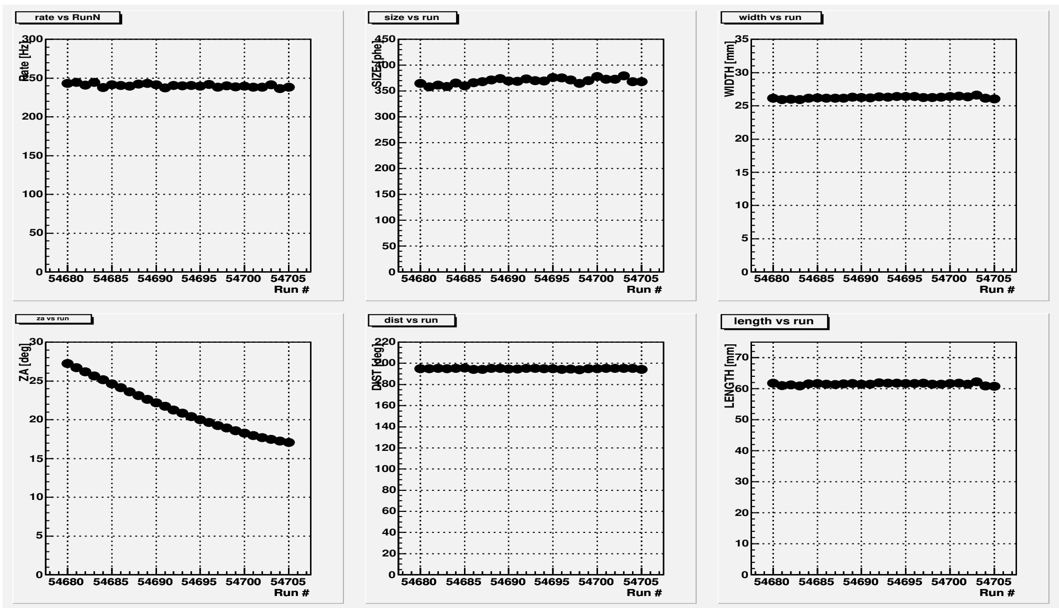

Figure 9: OFF sample (OffM87), May 6th (1.25 h). Plots of RATE, SIZE, WIDTH, ZA, DIST and LENGTH mean values. No SIZE cut.

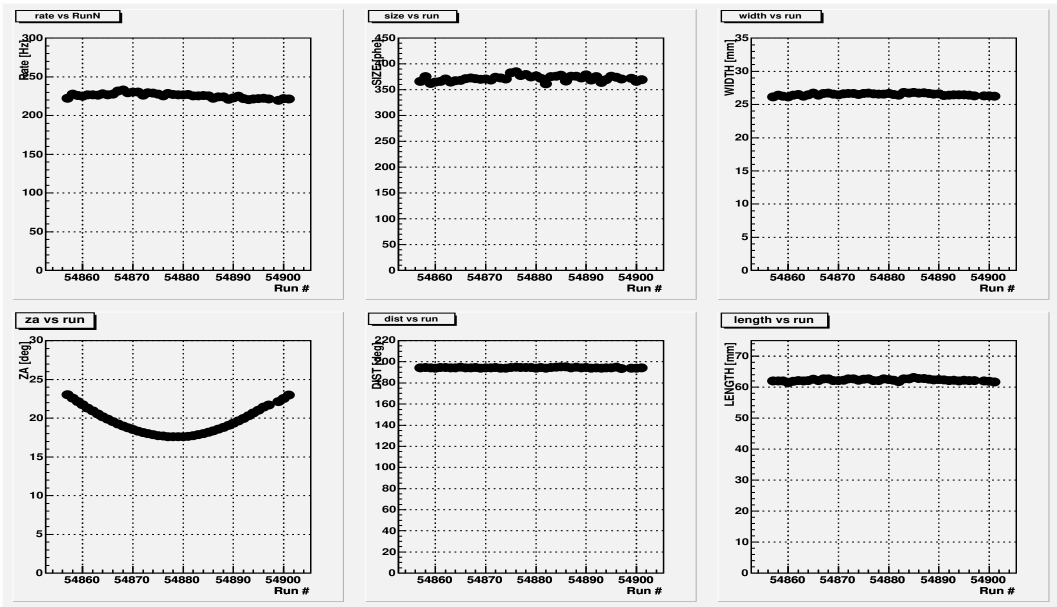

Figure 10: OFF sample (OffHB1553), May 7$^{\text{th}}$ (2 h). Plots of RATE, SIZE, WIDTH, ZA, DIST and LENGTH mean values. No SIZE cut.

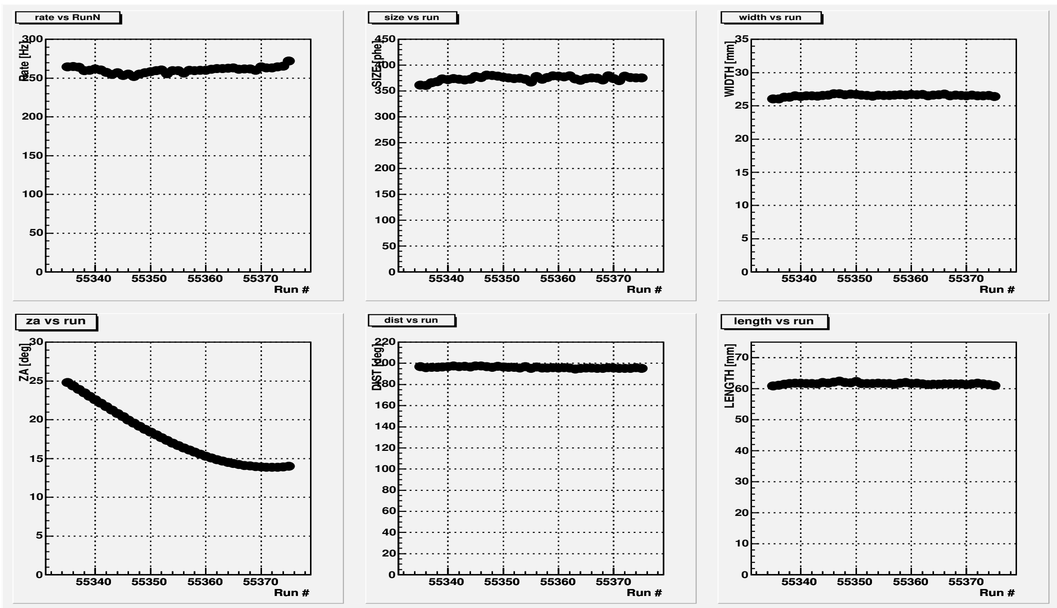

Figure 11: OFF sample (Off1ES1426), May 11$^{\text{th}}$ (2 h). Plots of RATE, SIZE, WIDTH, ZA, DIST and LENGTH mean values. No SIZE cut.

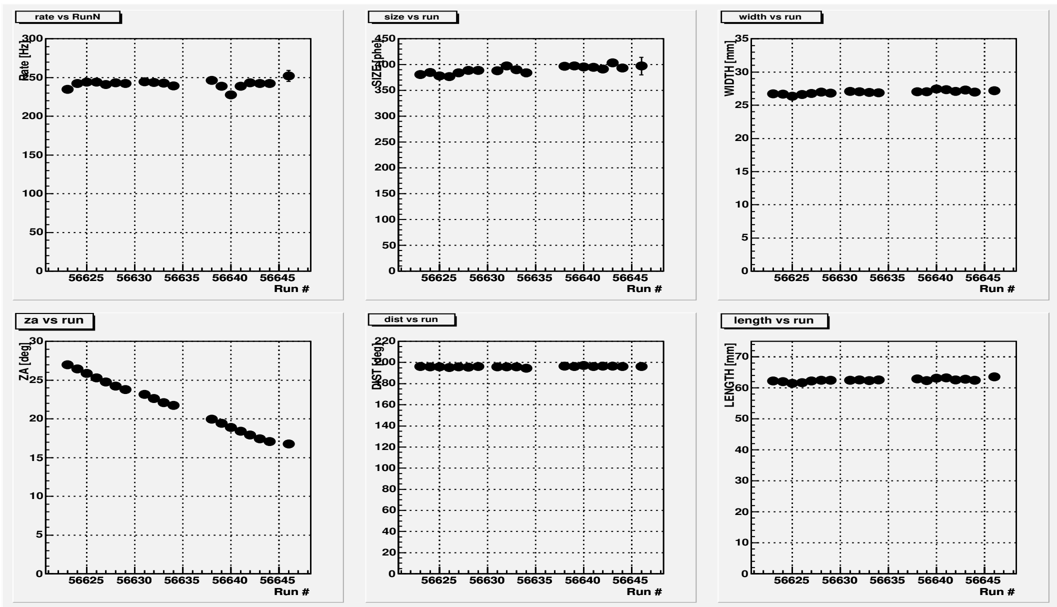

Figure 12: OFF sample (OffMrk501), May 30$^{\rm th}$ (0.8 h). Plots of RATE, SIZE, WIDTH, ZA, DIST and LENGTH mean values. No SIZE cut.

3.3 Data samples after run selection

After this preliminary checks the data samples which we decided to take into account are listed in table 3. We have plotted the SIZE, WIDTH, LENGTH and DIST distributions in order to compare ON and OFF sample. In figures 13 and 14, divided in two SIZE bins (100-400 phe- and 400-∞ phe-).

ON			OFF		
SOURCE	DAY	EFF. TIME (s)	SOURCE	DAY	EFF. TIME (s)
HB–1553	03	6147	OffM87-1	06	4531
HB–1553	09	3380	OffHB1553-1	07	7681
HB–1553	10	6033	Off1ES1426-1	11	6736
HB–1553	13	5668	OffMrk501-1	30	2987
		21228s (5.90 h)			21935s (6.09 h)

Table 3: Data sample used in the analysis. It is basically the initial data sample, without the bad runs of Day 10th for the ON and without the day 04th Mayfor the OFF.

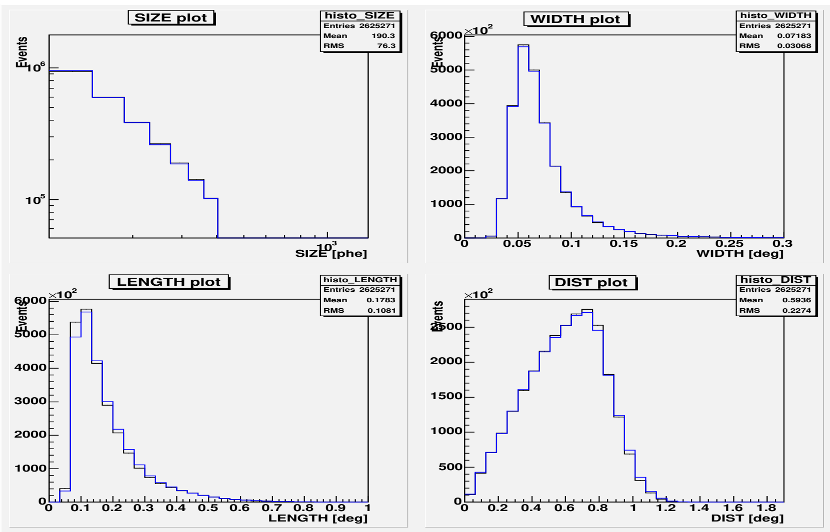

Figure 13: Hillas parameters comparison between ON (black) and OFF (blue) samples. 100-400 phe- SIZE bin.

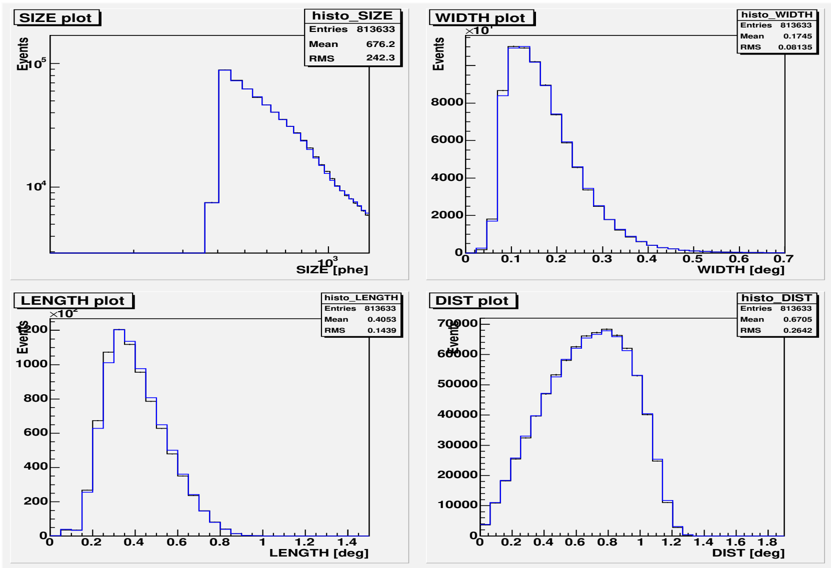

Figure 14: Hillas parameters comparison between ON (black) and OFF (blue) samples. 400-∞ phe- bin.

4 Camera inhomogeneities

We know from the work of P. Liebing [5], that the May data are heavily affected by the "pulse position" / camera inhomogeneity problem. Due to the different delays of the trigger macrocells, the position of the pulses in the FADC depends on the macrocell which fires the trigger. In some ocassions, and depending on the position of the image on the camera, the pulses are too early and are easily misreconstructed. This produces a deficit of events in some parts of the camera, as seen on a plot of the centers of gravity of images. Images on the right part of the camera (specially the upper right part) are the most affected by this problem, most clearly for small events since large events spill over other camera regions and the trigger is no longer given by the *bad* cells. The effect can be somehow mitigated by allowing the signal extractor to search for the pulse in a wider FADC range (in *Mars* terminology, switching off the "pulse position check"), and by using a "spline extractor" (which needs only that the peak of the pulse is within the FADC range and is unaffected by a partial truncation of the signal). Unfortunately in the May data the correction is more difficult since the *average* arrival time of pulses is already too early (see fig. 1), and when a *bad* macrocell triggers, pulses may go entirely out of the FADC range. The intensity of the effect changes from day to day (since it depends at least on the temperature of the electronics), which leads to differences between the data subsamples we have processed. The histogram of the center of gravity (COGs) of the images (15) shows that the upper-right region of the camera appears different for the OFF data (despite all the described corrections have been applied). The differences can be more easily seen in a ϕ plot (where ϕ is the azimuth of the image centroid with respect to the camera x-axis, fig.16.)   The distribution

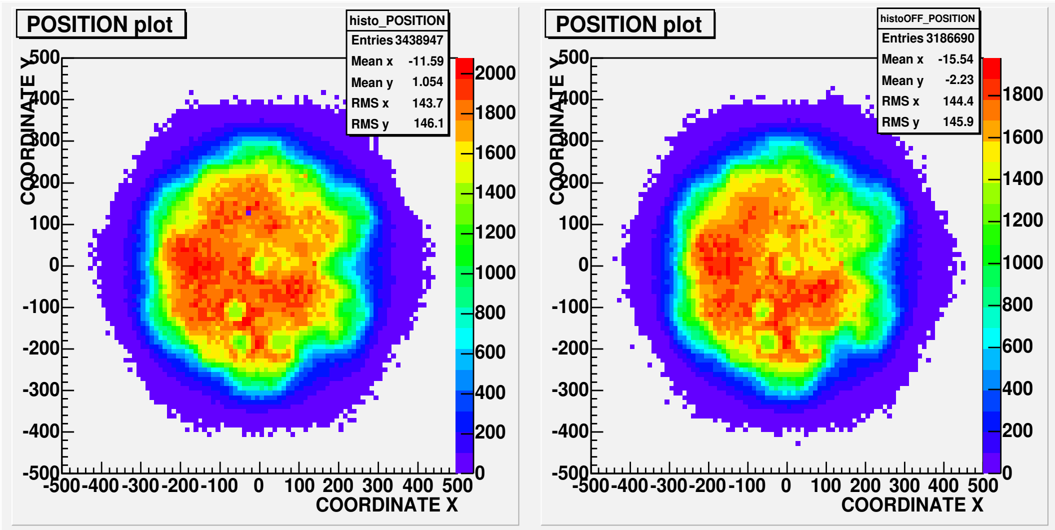

Figure 15: Mean image position plot comparison between ON (left) and OFF (right) samples.

around 50° is quite different for the ON and OFF samples. We made also some plots for the single OFF samples, and they show different features. A different distribution of the center of gravity of images produces a different alpha distribution for ON and OFF, making it more difficult to estimate, from the OFF data, the background in the ON sample. Not considering the events on upper-right region of the camera is the easiest way to cure those problems. The single OFF plots are shown in fig.17. The offMrk501 data sample taked at the end of the month (May 30$^{\rm th}$), is less affected by the inhomogeneities, as can be seen from the histogram in fig. 17. This means that the problem is almost solved at the end of the month. Unluckily this means that the end of May Mrk501 data we have used to optimize our cuts (see §6) is somehow different from the HB–1553 data. Despite this, the conservative cut to exclude the most affected region of the camera (see §5) should make the two datasets rather comparable.

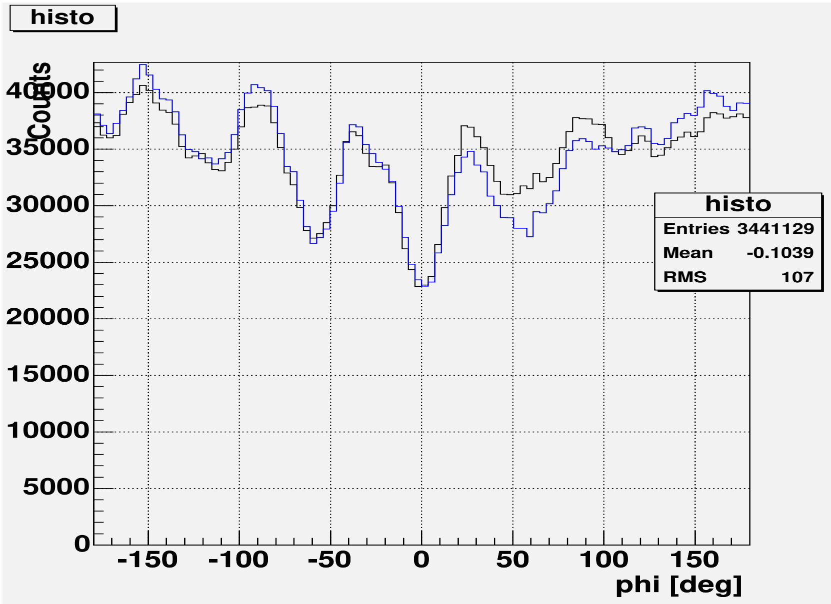

Figure 16: ϕ plot comparison between ON (black) and OFF (blue) samples. Cuts: SIZE $>$ 100 phe-, $0.19° < \text{DIST} < 0.96°$.

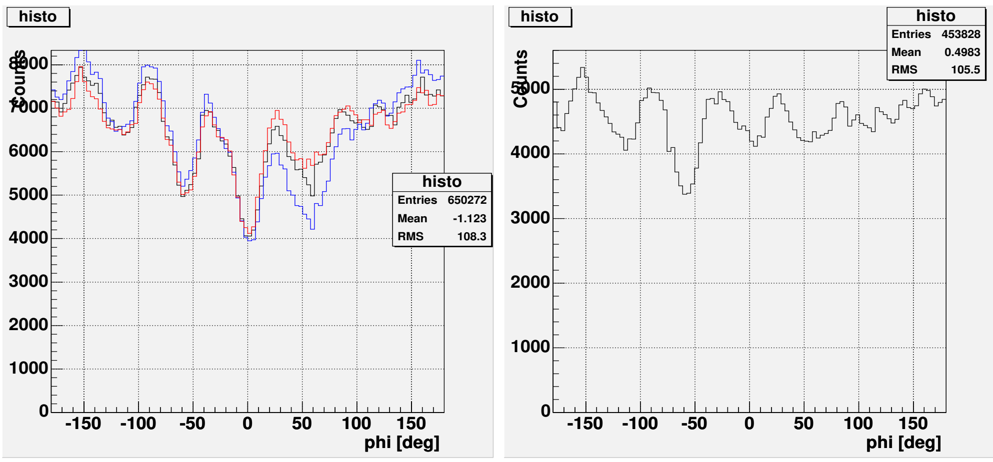

Figure 17: ϕ plots for the four OFF days considered. Left: OffM87 May 6^{th} (black), OffHB-1553 May 7^{th} (blue), Off1456 May 7^{th} (red). Right: OffMrk501 May 30^{th}. Cuts: SIZE>100 phe-, $0.19° < \text{DIST} < 0.96°$.

5 ALPHA distributions of ON and OFF data

To better understand if the OFF data we have is fully usable, we have plotted the ALPHA and abs(ALPHA) distributions for them and for the ON data after applying a set of basic quality cuts[3]. The following plots are made applying also a minumum SIZE $>$ 100 phe and $0.19° <$ DIST $< 0.96°$ cuts. We can see that excluding the top right region of the camera the agreement between ON and OFF is better, not only in the (-90;90) plot but also in the abs(ALPHA) plot, fig.18.
It is natural to get a slope in the ALPHA if part of the camera is excluded. The sign of ALPHA does not have a particular physical meaning, it is somehow related to where in the camera the image lies [6]. In the bottom plots of fig. 18 only the showers with COG in the top right region are considered. It may seem surprising that the agreement of the alpha distributions in that case is good, but note that the disagreement in the overall alpha plot of ON and OFF comes from the fact that there are fewer showers in the OFF coming from the upper right part of the camera (and hence their contribution to the slope of the overall alpha plot is smaller). When we separate the showers between those coming from the top right quadrant and the rest, and normalize OFF to ON in each of these two subsamples separatedly, the alpha shapes of ON and OFF agree well. In principle one can then use also the showers from the top-right quadrant as long as the normalization of ON and OFF is made separatedly for them, but in the present study we have decided conservatively to exclude them completely from the analysis.

Figures 19 and 20 are shown to highlight the different features of the available subsample of OFF data when no cuts are applied. In these detailed zoomed OFF plots of ALPHA (overlapped and normalized with the whole ON sample) we can see that the official OffHB1553 exhibits the bigger bias.

[3]Our quality cuts consists on: Spark events cut (excluding the population of odd events in the LogSIZE vs LogCONC plot), LEAKAGE $<$ 0.1 and minimum number of core pixels used $>$ 4.

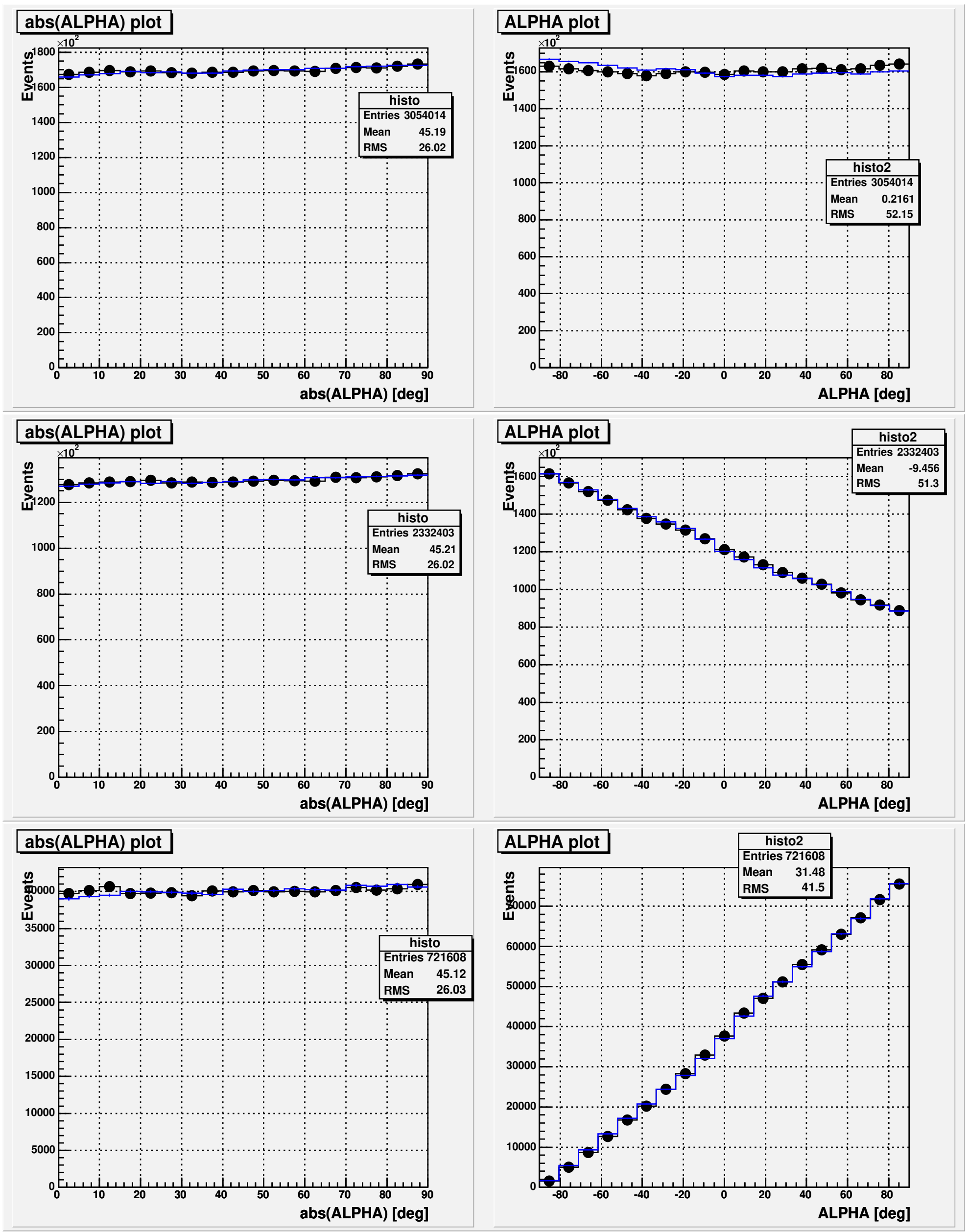

Figure 18: ALPHA plots comparison between ON (black) and OFF (blue) samples. Here no HADRONNESS cut is apply only SIZE > 100 phe and 0.19° < DIST < 0.96° cuts. In the first row no further cut are applied, in the second the top-rigth region of the camera is excluded and the third one is built with only the top-right sector of the camera.

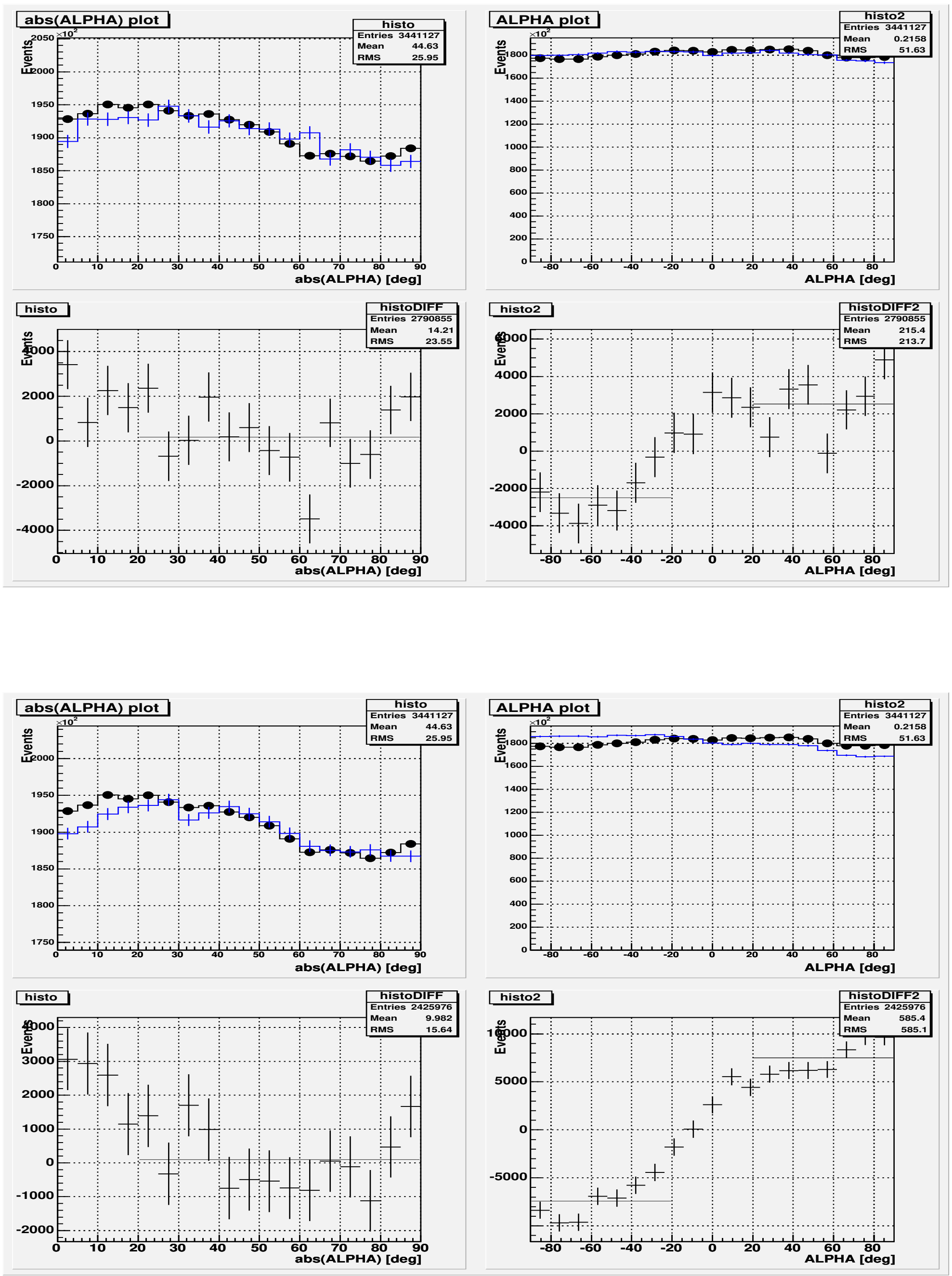

Figure 19: The black dots represent the whole ON sample considered, which is the same in the four plots. The blue lines represent the single OFF distributions. This is to highlight the difference between the four OFF considered and the ON. Top: OffM87 May 6$^{\mathrm{th}}$, bottom: OffHB-1553 May 7$^{\mathrm{th}}$

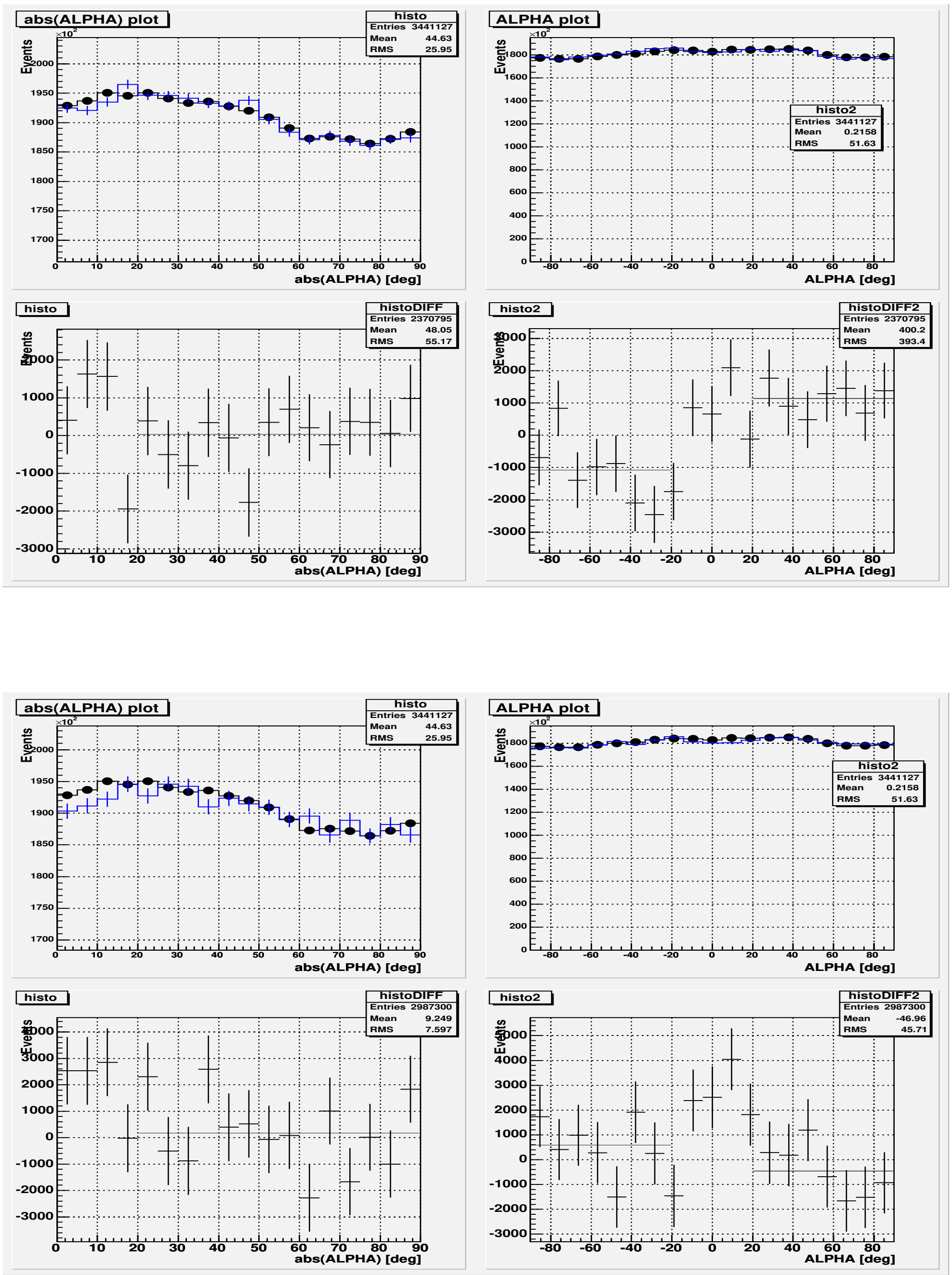

Figure 20: The black dots represent the whole ON sample considered, which is the same in the four plots. The blue lines represent the single OFF distributions. This is to highlight the difference between the four OFF considered and the ON. Top: Off1456 May 11th, bottom: OffMrk501 May 30th. Note the zoom in the Y axis. Cuts: SIZE $>$ 100 phe, $0.19° <$ DIST $< 0.96°$.

6 Analysis

For the γ/hadron separation the Random Forest (RF) method has been used. It requires two training samples, of gammas and hadrons respectively. The gamma train sample consists of 48842 MC events (SIZE>100 phe). The γ-s have been simulated with an global optical PSF of $\sigma = 0.053°$, by adding at the camera simulation level an additional spread of $\sigma = 14$ mm (in each axis) to the arrival position of photons in the camera. The zenith angle bins used are from 5 to 12 that correspond to 18-28° of ZA. Two thirds of all the available MC gammas are used for training the random forest, the remaining third as test sample.

Concerning the hadron train sample, a blend of randomly chosen ON and OFF real events has been taken, for a total amount of $5 \cdot 10^4$ events. The tiny "contamination" of gamma rays from the source that might be contained in this sample is too small to pose a problem to the training. After all, even in a sample of pure OFF data there will be some electromagnetic showers originated by electrons, or hadron-initiated showers which are dominated by a single electromagnetic shower (at least for what concerns to the light seen by the telescope). These showers probably outnumber the ones initiated by gammas from the studied sources, except for the strongest ones, and so a subsample of the ON data can be included among the training hadrons. This has the advantage that these real data have exactly the same characteristics (determined by weather, telescope conditions, etc) as the background events we want to supress.

The first analysis step is the building of the RF matrix using the *osteria* executable. Here we already applied a set of preliminary cuts as: the SPARK EVENTS cut, SIZE> 100 phe, Number of Core Pixels > 4 and LEAKAGE1<0.1. These are just basic quality (or "filter") cuts to ensure that the images are due to showers, large enough to obtain from them meaningful moments, and well contained in the camera. We have then used two different approaches: a DISP-based analysis and a more traditional ALPHA-based analysis. The former will be presented in the following, while the latter can be found in an appendix at the end of the note [4].

The parameters selected to be used in the RF trees (i.e. the separat-

[4] In the alpha-based analysis, where source-dependent parameters like DIST are used, we accidentally forgot to include the sign of M3LONG (third moment along main image axis) referred to the nominal source position (in *Mars* terminology, $fM3Long \times sign(fCosDeltaAlpha)$), and hence its discrimination power is significantly reduced. On the other hand, in the DISP-based analysis, this third momentum discrimination is "automatically" done at the moment of deciding the head and tail of the shower. So we expect our DISP-based analysis to be somewhat more sensitive than our alpha analysis.

ing parameters) are: Log(SIZE), WIDTH, LENGTH, AREA ($WIDTH \times LENGTH$), and CONC (ratio between signal in two highest pixels and SIZE). Then every event is tagged with the well known HADRONNESS coefficient using the *melibea* executable. The DISP values are computed with the specific options available for the *osteria* and *melibea* executables[8].

We decided a priori three SIZE (phe) bins where look for a signal. We chose: SIZE > 100, SIZE > 300 and 100 phe $<$ SIZE $<$ 500 phe. The first two bins correspond to two integral SIZE bins with two different lower thresholds, the former (>100 phe) corresponds to what we think is the MAGIC performance limit for that period. The latter (>300 phe) correspond to an energy bin where we suppose the analysis works optimally and the sensitivity (in terms of Crab units) reaches its best, of around 2.5 percent of Crab in a 50 hours observation. The third bin (100 phe $<$ SIZE $<$ 500 phe) is somehow tied to the features of this potential source: models predict an energy cut-off for such a far source at about 200 GeV (assuming a redshift of $\sim$0.35), due to the absorption on the EBL (Extragalactic Background Light). For the case of weak sources it is particularly important to choose in advance the data samples which will be tested for a possible signal, to avoid tuning *a posteriori* the cuts (in SIZE or whatever) on the real data, which may lead to an overestimation of the signal. The plots in 21 shows what are our MC-γ peak energies for the three selected size bins and for a sample with a lower size cut of 500 phe, in which we can see that very few events below 200 GeV survive. With exactly the same procedure, but of course with a specific RF training (due to a different hadron training sample), we analysed also about 2 hours of Markarian 501 data taken on May 29^{th} and June 1^{st}. The flux level was roughly 30% of Crab flux and even if those data are not exactly in the same period of the HB-1553 sample (already at the end of May the detector conditions were different, see §4), they are the closest data with a clear signal. We did not choose the 1st July Mrk501 flare data because even if more rich in gammas, they are more distant in time. We also prefer to use data from Mrk501 in a lower state than it was during the July 1^{st} flare, since the goal is to optimize the hadronness cuts for the analysis of HB-1553. Having a large absolute flux, with many high energy events, the optimization of cuts on the flare data might not be ideal for a source with no (or very few) expected events at large energies.

In the following section we will always show the HB-1553 θ^2 plots and also the corresponding Mrk501 ones. On using a reference source, or even MC gamma events, to optimize the hadronness cut, first one has to decide what will be considered as the optimal cut. A rather natural choice may be the one which maximizes the statistical significance of the detection (doing so, obviously, for the reference source). On the other hand, this is not the only

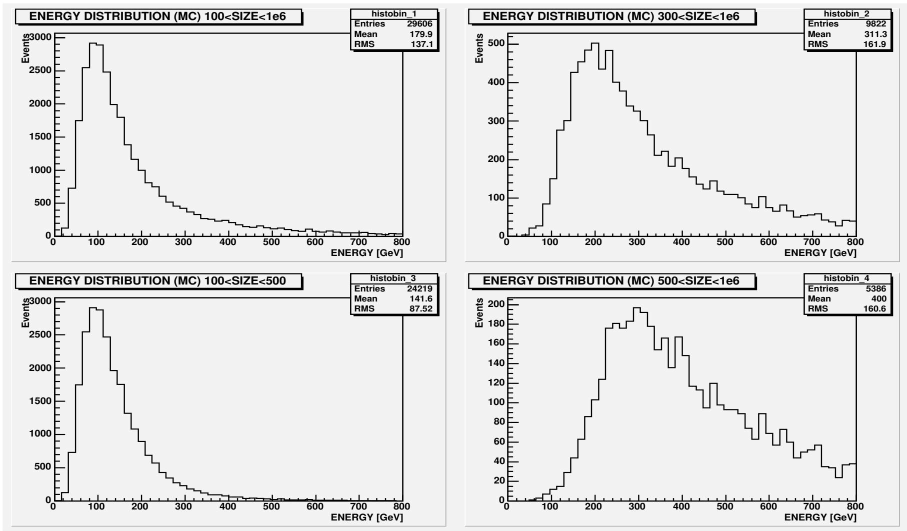

Figure 21: Real (MC) Energy γ distributions for the three size bins used and for a SIZE bin with 500 phe like lower limit (in this last case most part of the events have energy above 200 GeV).

reasonable criterium; for the case of a weak source, it may be better to choose the cuts which maximize the ratio of the number of excess events over the number of residual background events. Even if it results in a lower statistical significance, this approach may result in a more "convincing" excess. The reason is that a signal of large significance may come from a bias in the estimation of the background. If the background is large, a bias of just a few percent may result in a (fake) statistically significant excess of events. So for small signals we may have more trouble with possible systematics in the background determination than with the pure background fluctuations (also because the latter may be reduced by enlarging the observation time, while the former become even more difficult to keep under control for long observational periods).

In the present study the HADRONNESS cuts have been optimized in two different ways:

- We used the MC-γ files to simulate the signal and our real OFF as background, and then determined the HADRONNESS cut which maximized the significance (computed by the approximate formula $EXC/\sqrt{ON+OFF}$ formula)[5]. As an additional constraint we required a gamma efficiency

[5]This simplified expression has been employed only for the cut optimization; final significances of the excesses are computed with formula 17 from Li & Ma[7]

ϵ_γ of at least 30% (where ϵ_γ is the ratio: $\gamma_{survived}/\gamma_{initial}$). This is somehow an arbitrary choice, but for a weak source some requierement of this sort is needed to avoid being left without signal (which is not an issue in the case of the MC gamma since we start with several tens of thousands of events).

- We used Mrk501 real data as ON and the relative OFF as background. In this case we found the HADRONNESS cut which optimized the EXCESS/BACKGROUND ratio for the Mrk501 data. The Mrk501 optimal HADRONNESS cut value is not directly applied to HB-1553 datas because the RF matrixes are different for the two sources (due to the different training hadron samples). The optimal Mrk501 cut is "translated" to HB-1553 by the gamma efficiency (tuning the HADRONNESS cut till have the same ϵ_γ).

The final significances are computed with the formula 17 from Li & Ma[7]. It was not possible normalize the OFF distributions to the ON using the Effective Time (ET). Using the ET_{ON}/ET_{OFF} (2.1228 s/2.1935 s) normalization coefficient, the distributions do not match by about ∼20%. This points at some systematic difference in the rates of the ON and OFF observations after all cuts, but until now it has not been possible to further investigate the reason for it. The ratio used to normalized the distribution is the fraction between the numbers of events (#ON/#OFF) at $\theta^2 > 0.1\text{deg}^2$ (or at ALPHA $> 25°$ for the alpha analysis).

7 Results of θ^2 analysis

TABLE OF σ				
SIZE bin (phe)	HB-1553 (MC opt.)	Mrk501 (MC opt.)	HB-1553 (Mrk501 opt.)	Mrk501 (Mrk501 opt.)
SIZE>100	2.42	9.39	1.58	7.50
SIZE>300	2.89	9.55	1.30	7.41
100<SIZE<500	3.94	4.37	1.81	3.32

Table 4: Summary table of significance (formula 17 Li & Ma) values obtained.

7.1 SIZE > 100 phe bin

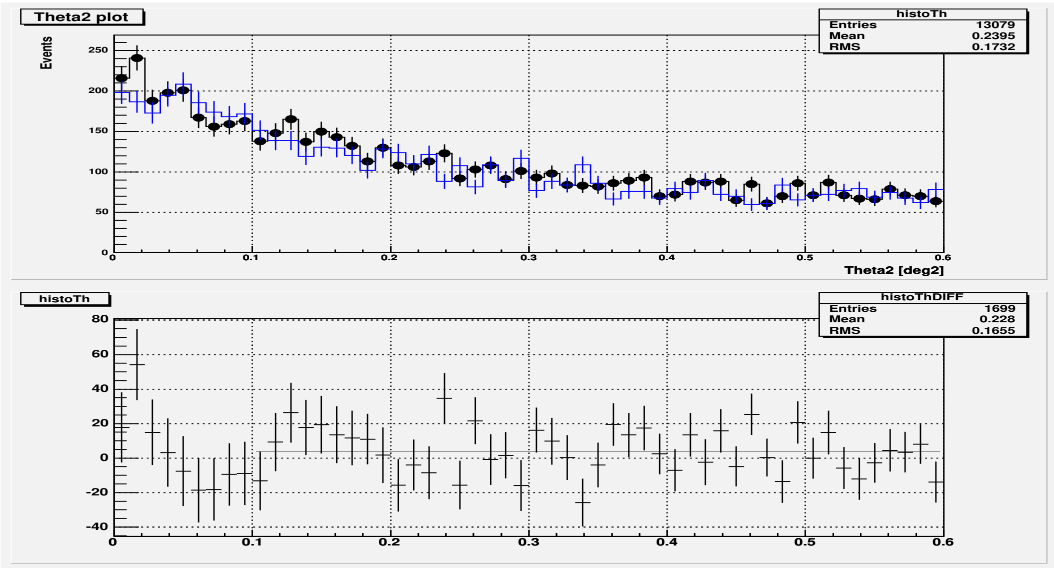

Figure 22: **HB-1553** (σ = 2.42 [LiMa 0.033 deg]) optimize using MC gamma. Common cuts & SIZE>100 phe & HADR.<0.025.

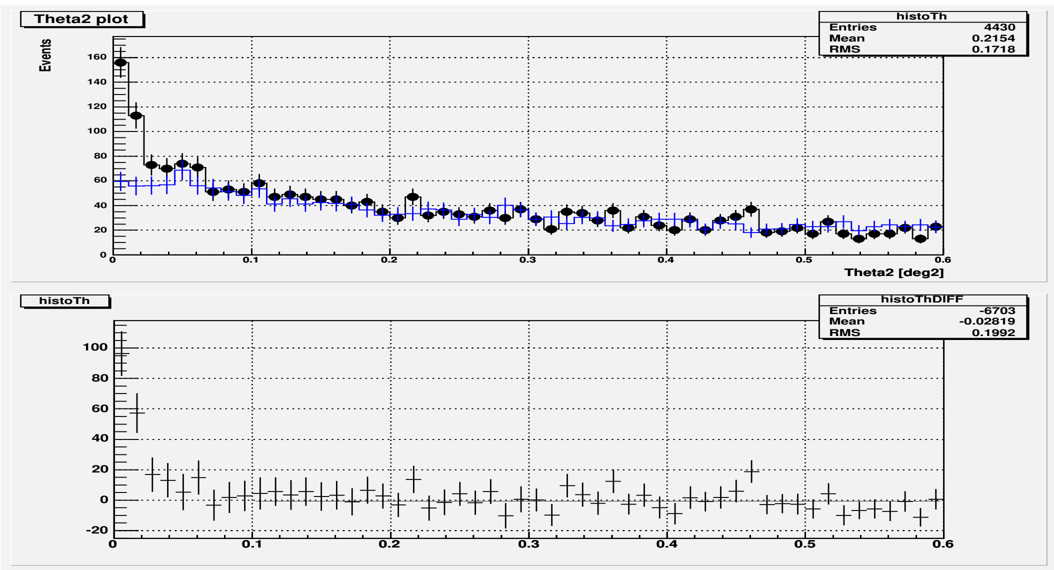

Figure 23: **Mrk501** (σ = 9.39 [LiMa 0.033 deg]) optimize using MC gamma. Common cuts & SIZE>100 phe & HADR.<0.025.

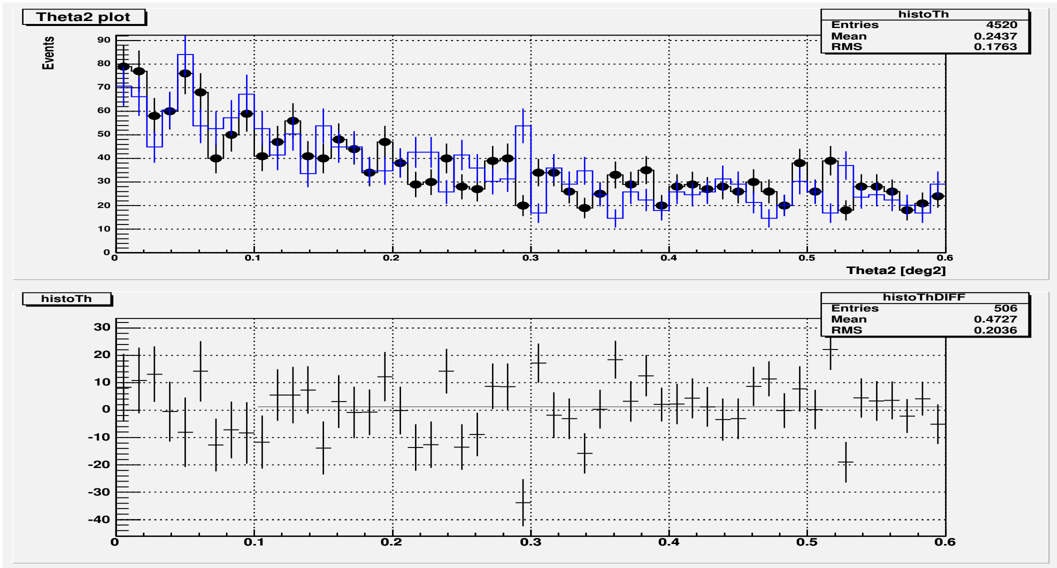

Figure 24: **HB-1553** (σ = 1.58 [LiMa 0.033 deg]) optimize using Mrk501. Common cuts & SIZE>100 phe & HADR.<0.01.

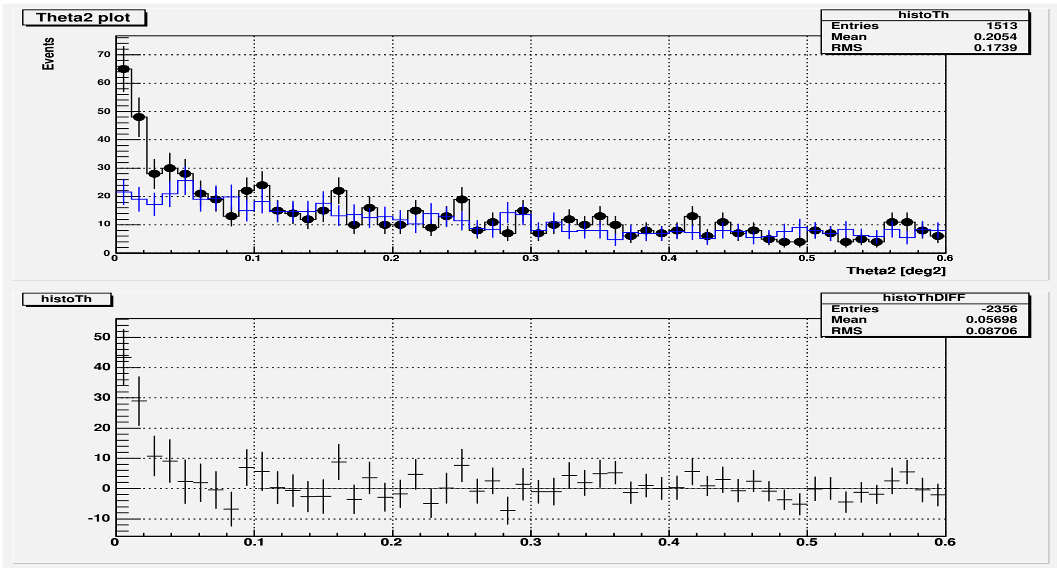

Figure 25: **Mrk501** (σ = 7.50 [LiMa 0.033 deg]) optimize using Mrk501. Common cuts & SIZE>100 phe & HADR.<0.01.

7.2 SIZE > 300 phe bin

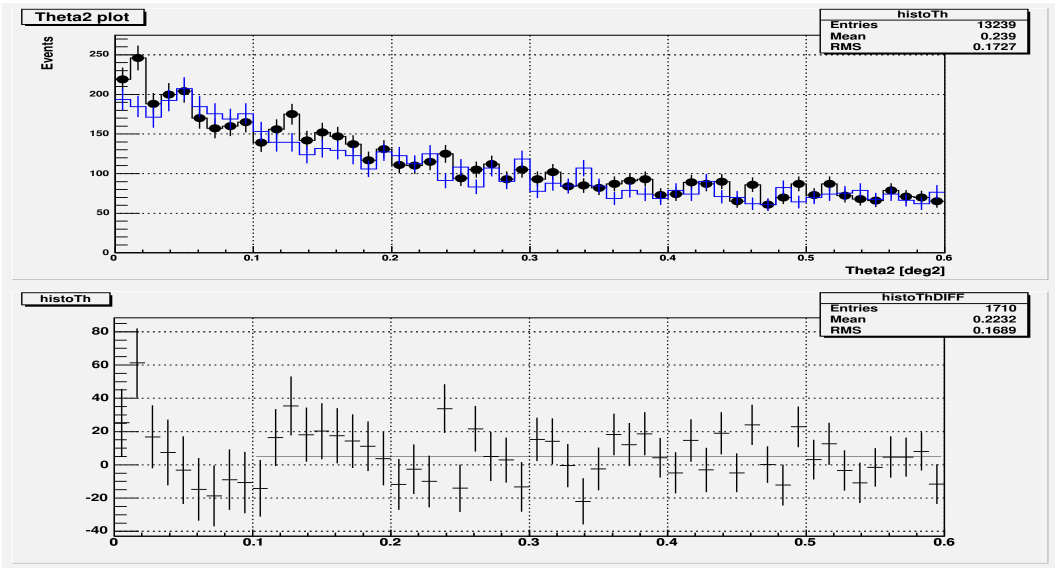

Figure 26: **HB-1553** (σ = 2.89 [LiMa 0.033 deg]) optimize using MC gamma. Common cuts & SIZE>300 phe & HADR.<0.03.

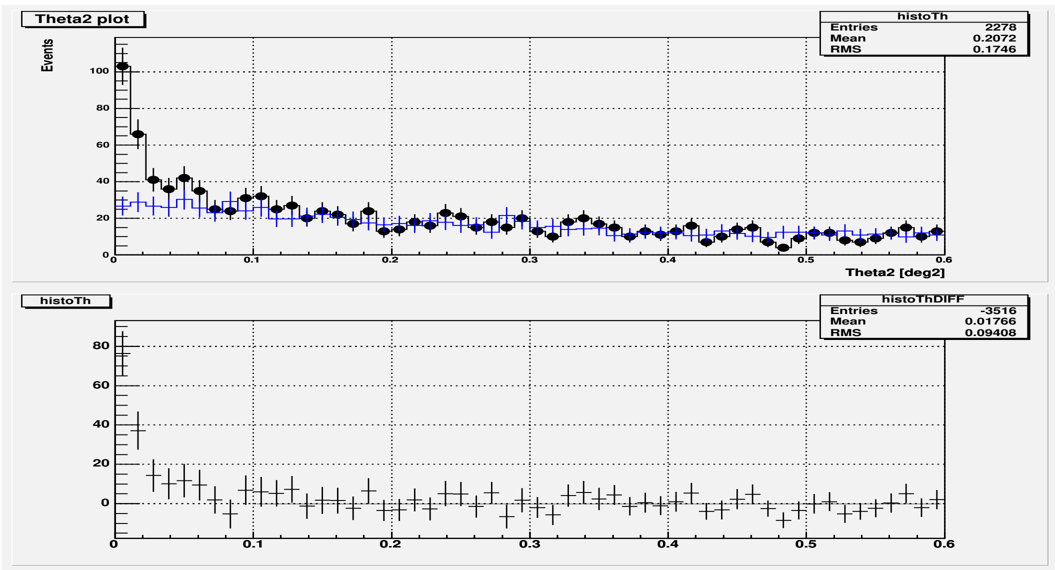

Figure 27: **Mrk501** (σ = 9.55 [LiMa 0.033 deg]) optimize using MC gamma. Common cuts & SIZE>300 phe & HADR.<0.02.

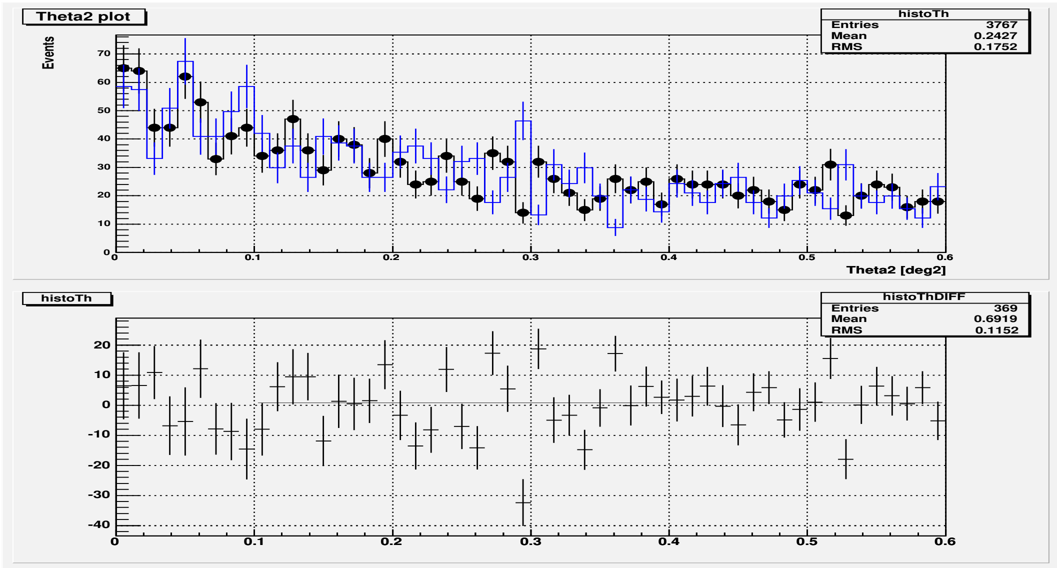

Figure 28: **HB-1553** (σ = 1.30 [LiMa 0.033 deg]) optimize using Mrk501. Common cuts & SIZE>300 phe & HADR.<0.03.

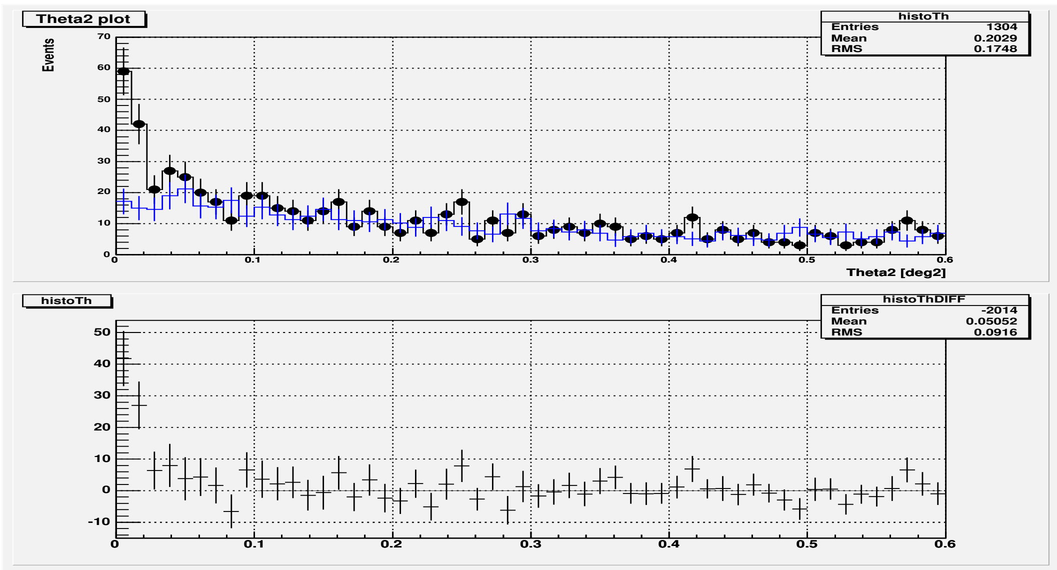

Figure 29: **Mrk501** (σ = 7.41 [LiMa 0.033 deg]) optimize using Mrk501. Common cuts & SIZE>300 phe & HADR.<0.01.

7.3 100 phe < SIZE < 500 phe bin

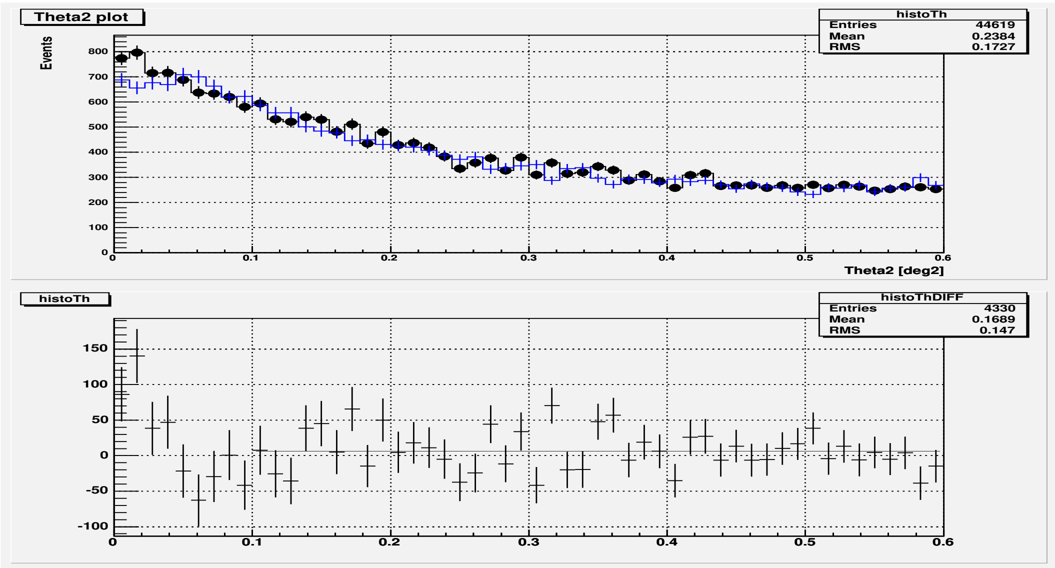

Figure 30: **HB-1553** (σ = 3.94 [LiMa 0.033 deg]) optimize using MC gamma. Common cuts & 100 phe<SIZE<500 phe & HADR.<0.085.

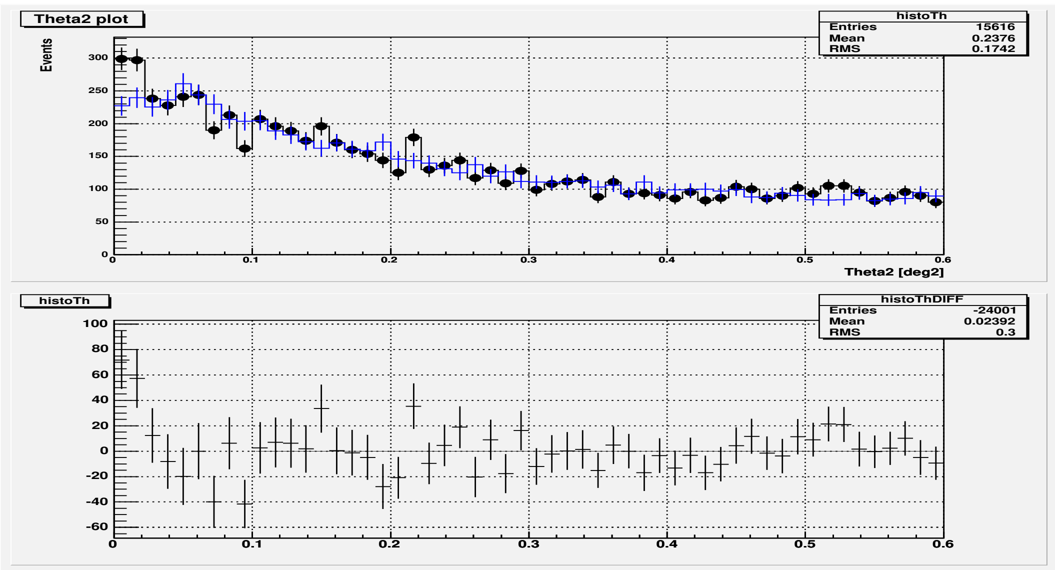

Figure 31: **Mrk501** (σ = 4.37 [LiMa 0.033 deg]) optimize using MC gamma. Common cuts & 100 phe<SIZE<500 phe & HADR.<0.085.

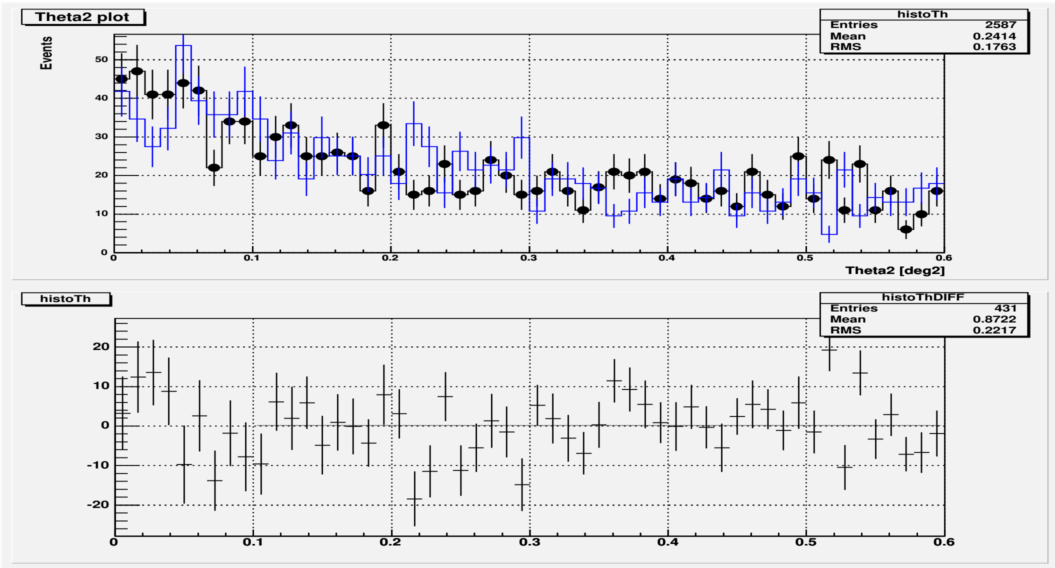

Figure 32: **HB-1553** (σ = 1.81 [LiMa 0.033 deg]) optimize using Mrk501. Common cuts & 100 phe<SIZE<500 phe & HADR.<0.01.

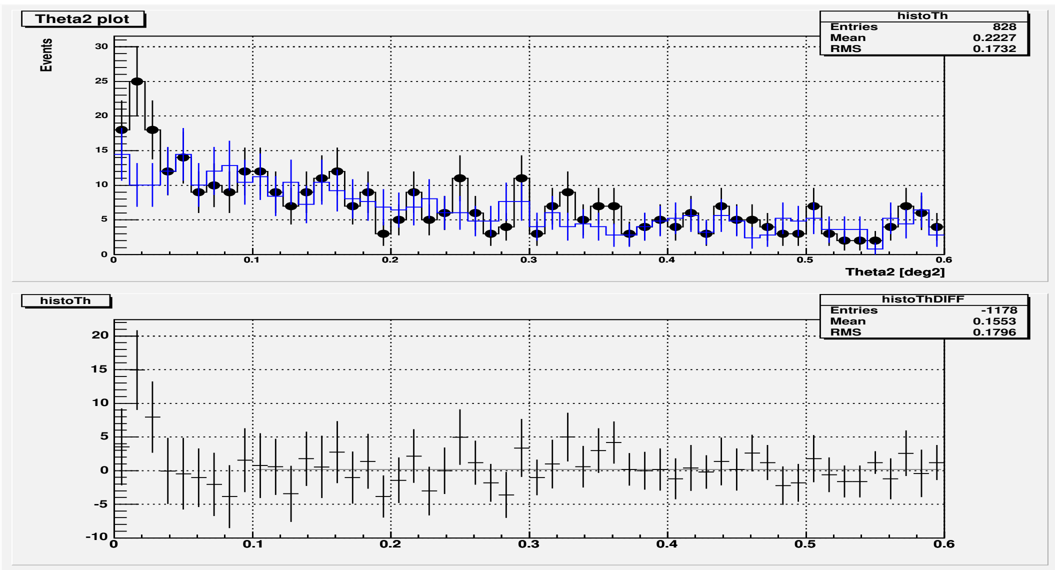

Figure 33: **Mrk501** (σ = 3.32 [LiMa 0.033 deg]) optimize using Mrk501. Common cuts & 100 phe<SIZE<500 phe & HADR.<0.01.

8 Conclusions

The analysis of the HB89-1553+11 May data with the RF method presented in this report has produced inconclusive results. There are some hints of a signal, but on the other hand the observations were not performed during a period of optimal telescope performance. It may well be that these hints are really due to gamma rays from the source (specially given that HESS has detected this source, though at a very low flux level of about 2% of Crab above 200 GeV), but in our opinion the evidence is not yet strong enough as to safely claim a detection. We have to note that the clearest excesses in the θ^2 plots results mainly from a flattening of the OFF distribution towards low values of θ^2. This of course does not mean that that the excess is not due to gammas, but only that it is somewhat supicious and we have to be careful about it. In different OFF data we have seen as well θ^2 distributions which keep on raising towards $\theta^2 = 0$, much like the ON data of the source we are dealing with. Furthermore the ON and OFF matching is not perfect, though acceptable after the cuts we have imposed (mainly the exclusion of images with c.o.g. in the upper right quadrant of the camera). So, we cannot guarantee the absence of any bias which may be faking the excess. The fact that the normalization of ON to OFF using effective observation times does not work (by about 20%) is also a hint that something may not be working fine.

We have also to take into account that, at least at the beginning, and statistically speaking, this was not a "single test". Originally, we looked deeper into this source because a previous analysis (from the Würzburg group) already revealed some hints of signal in it. But in the Würzburg Data Center many sources have been analyzed, and we did not choose this one randomly from the whole object sample. Now this argument can be turned upside down after the HESS detection, since this source has been singled out by having been seen by an independent experiment. On the other hand, we tried several ways to optimize the cuts and two different approaches to the analysis (θ^2-based and alpha-based - see appendix), plus three different SIZE bins, and we have obtained quite a range of different excesses (always positive, though). We should avoid picking up the most significant one (3.94 σ) and wave it as the result of this work. These multiple trials should be taken into account when assessing the real significance of the results presented here (see 34).

This may be a source at the edge of our sensitivity (for the given observation time), as it would be the case if the flux reported by HESS was the one during MAGIC observations.

We should be careful not to tune the cuts on the data or pick up arbitrarily

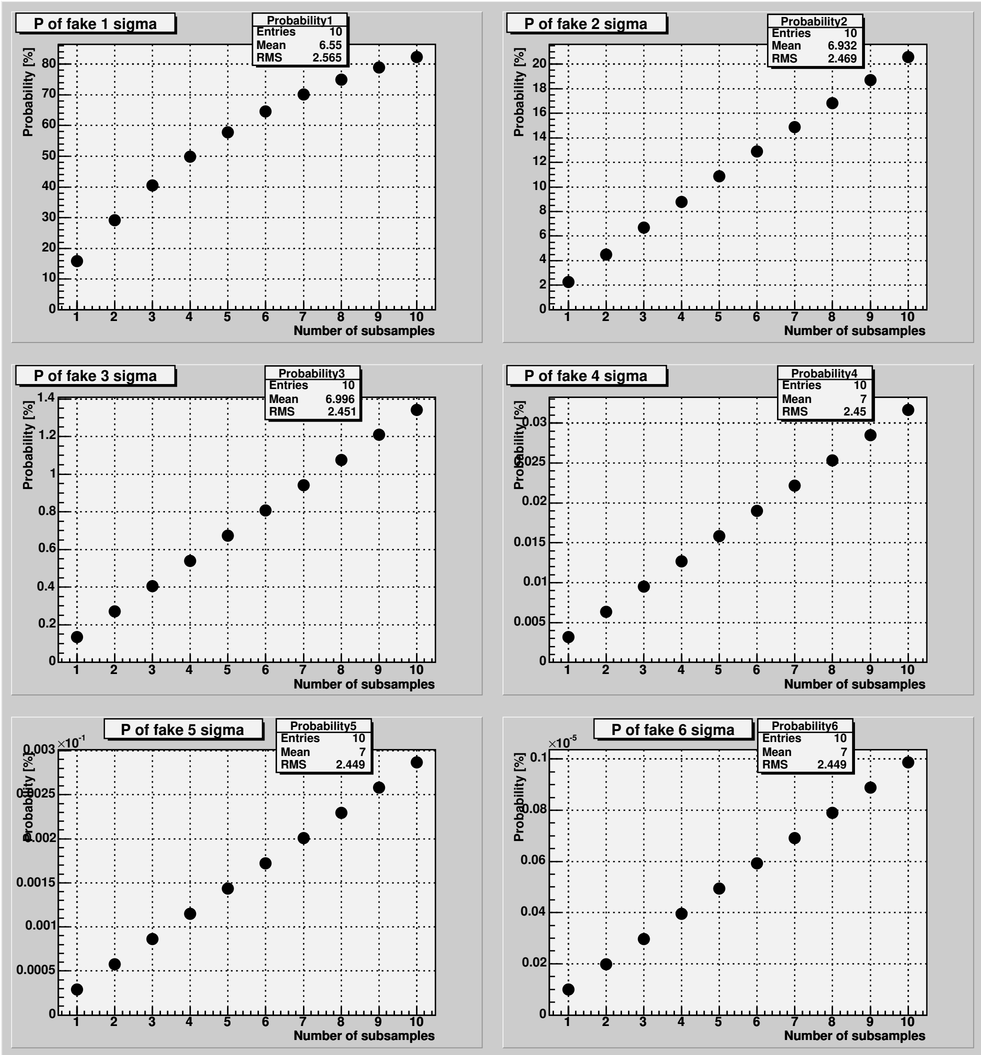

Figure 34: Probability that an n-sigma signal is due to a pure statistical fluctuation as function of the number of test made.

the largest excesses, because this is bound to result in a wrong flux.

Work is in progress to improve the sensitivity with the help of a time image cleaning and some time parameters. If results show an improvement in the performance, it is our intention try to re-analyze in this way the HB-1553 data sample. In any case the preliminary results obtained fully justify further observations of this source. If we assume an excess of 3 σ in our current data, 18 h of observation (three times our actual ON sample) should produce a signal of roughly 5.2 sigma (assuming the same flux level), that would be a safe evidence of detection, and would permit a more detailed analysis.

A Results of ALPHA analysis

TABLE OF σ				
SIZE bin (phe)	HB-1553 (MC opt.)	Mrk501 (MC opt.)	HB-1553 (Mrk501 opt.)	Mrk501 (Mrk501 opt.)
SIZE>100	2.96	9.65	0.13	6.15
SIZE>300	2.75	7.91	0.05	6.68
100<SIZE<500	2.75	4.92	1.49	4.38

Table 5: Summary table of significance (formula 17 Li & Ma) values obtained.

A.1 SIZE > 100 phe bin

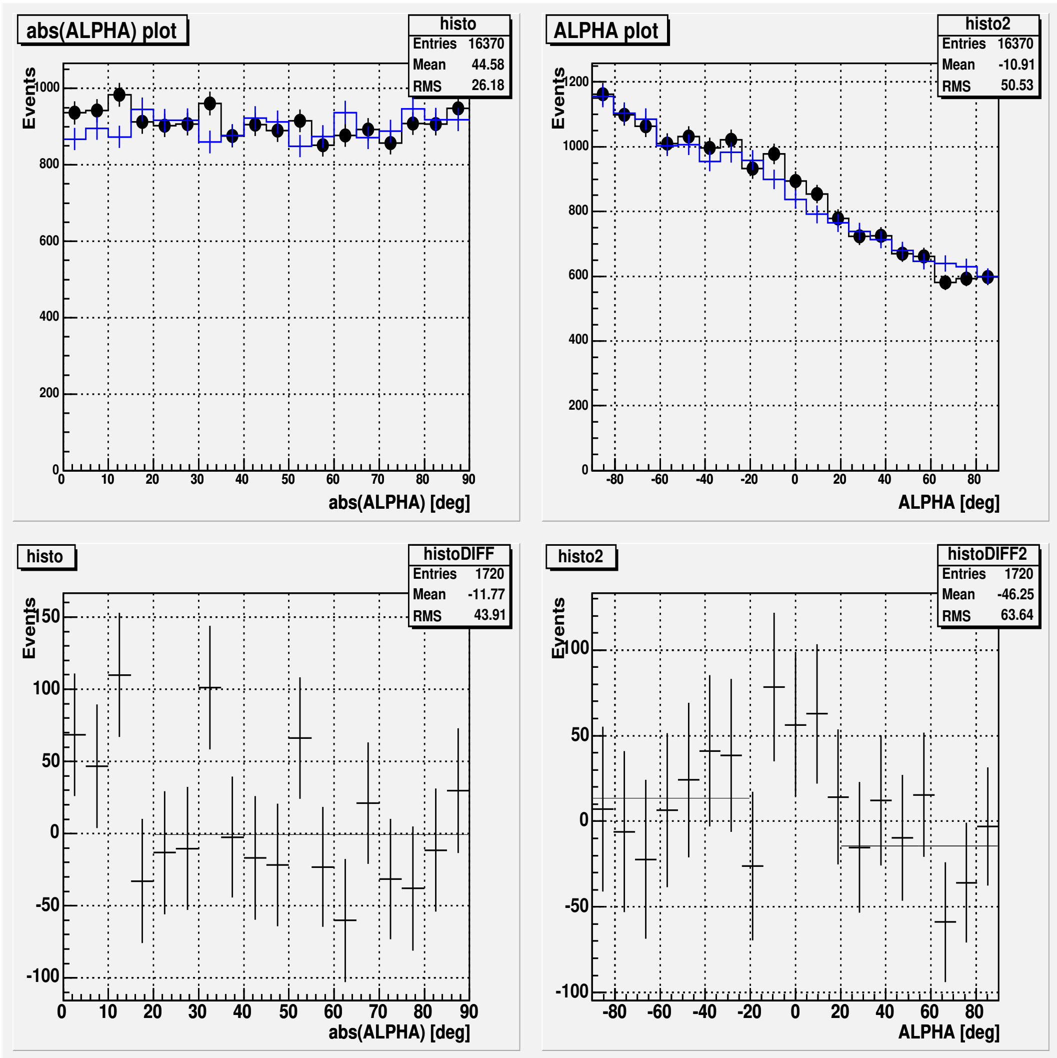

Figure 35: **HB-1553** ($\sigma = 2.96$ [LiMa 15deg]) optimize using MC gamma. Common cuts & SIZE>100 phe & HADR.<0.05.

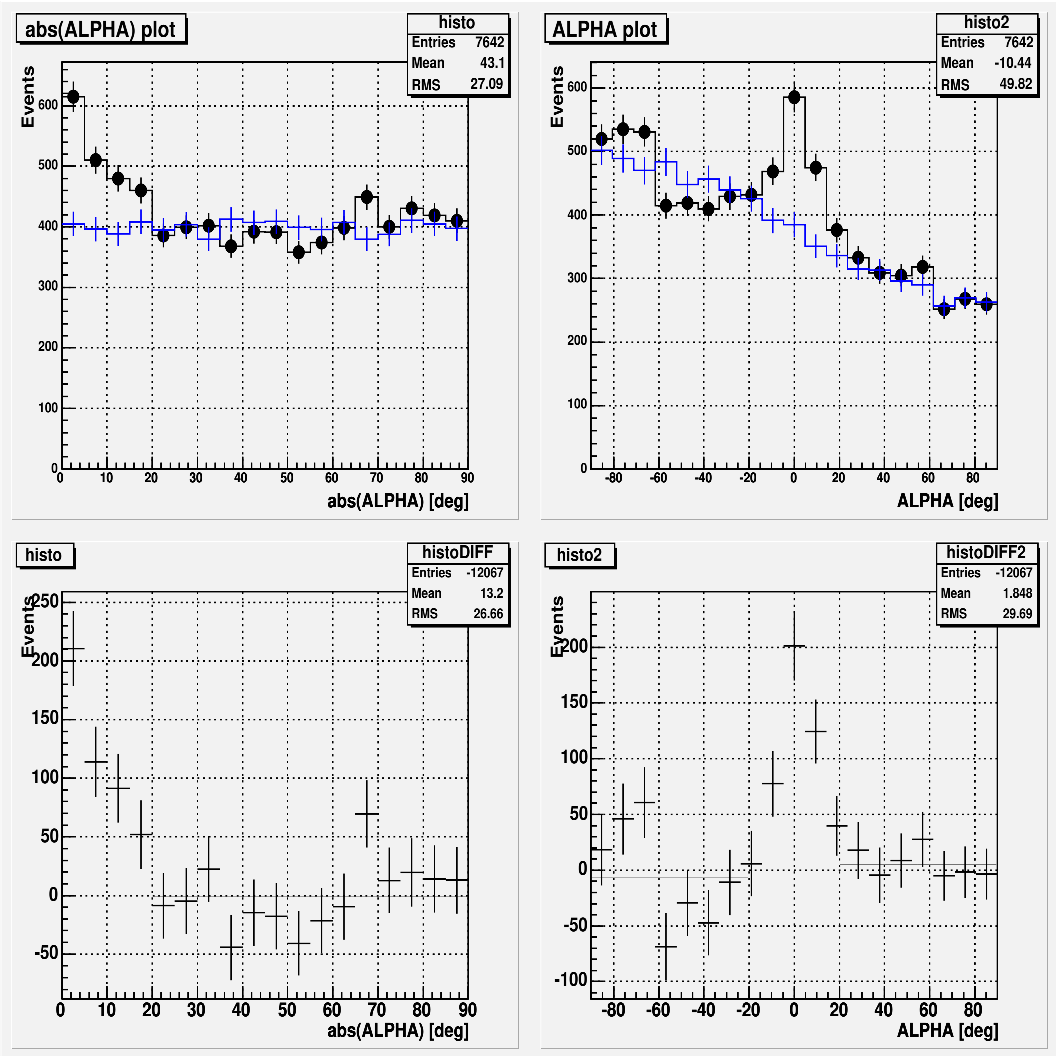

Figure 36: **Mrk501** (σ = 9.65 [LiMa 15deg]) optimize using MC gamma. Common cuts & SIZE>100 phe & HADR.<0.045.

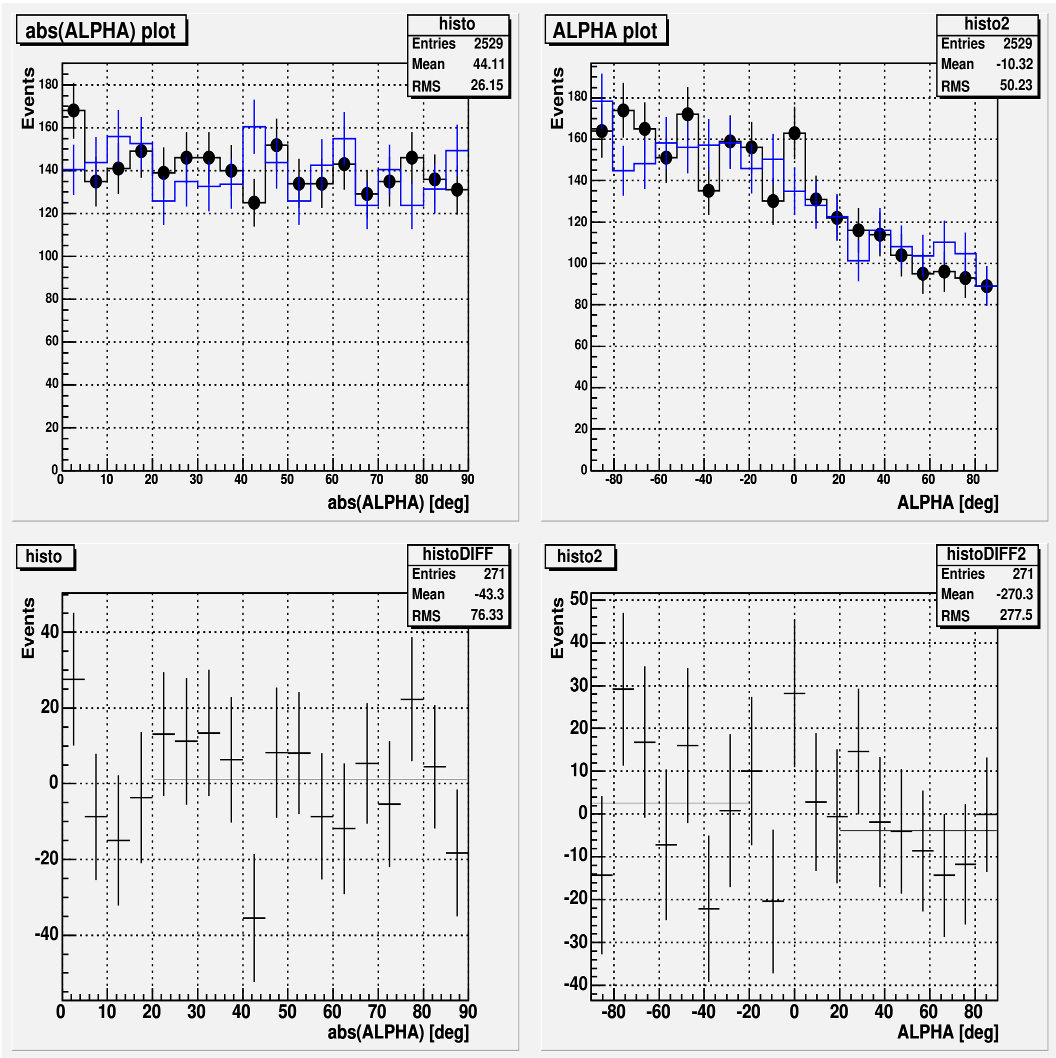

Figure 37: **HB-1553** (σ = 0.13 [LiMa 15deg]) optimize using Mrk501. Common cuts & SIZE>100 phe & HADR.<0.01.

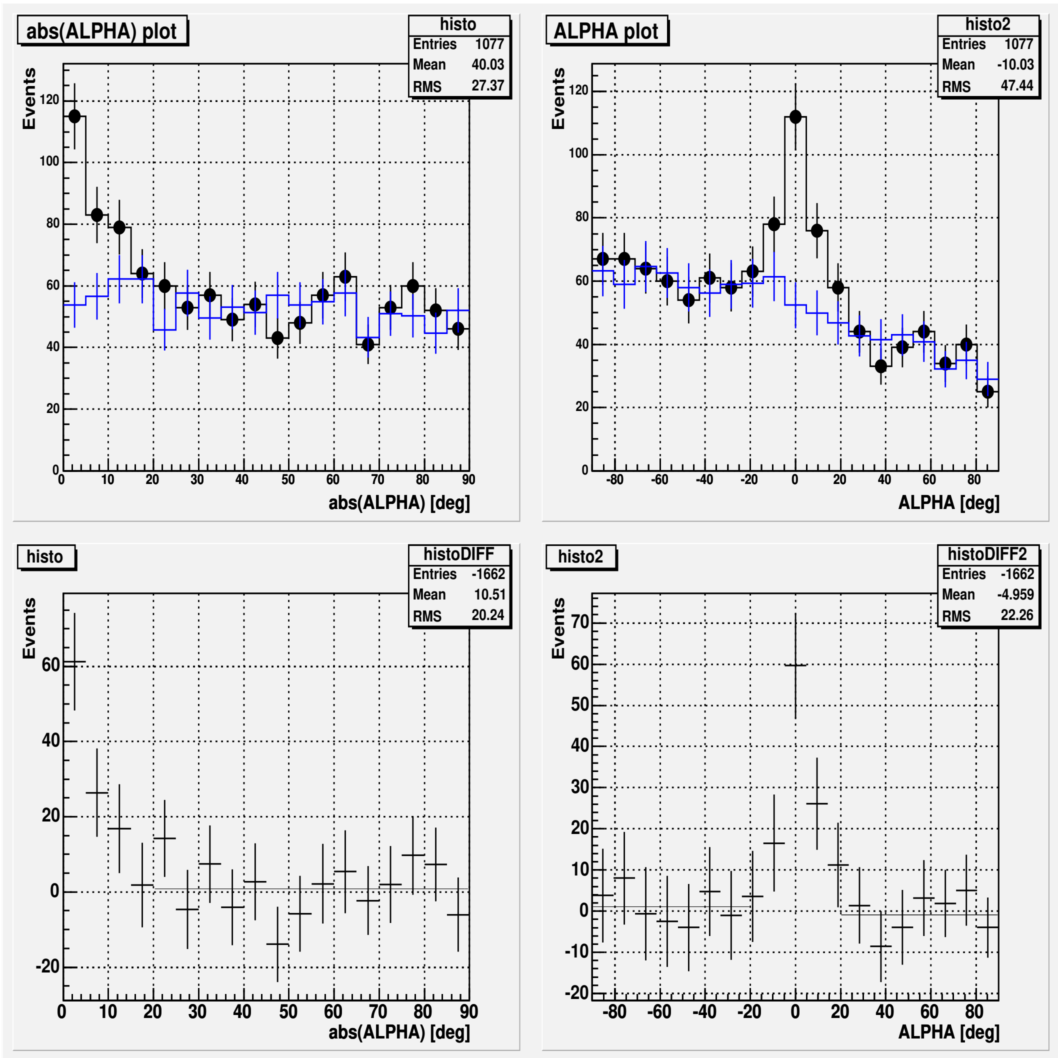

Figure 38: **Mrk501** ($\sigma = 6.15$ [LiMa 15deg]) optimize using Mrk501. Common cuts & SIZE>100 phe & HADR.<0.005.

A.2 SIZE > 300 phe bin

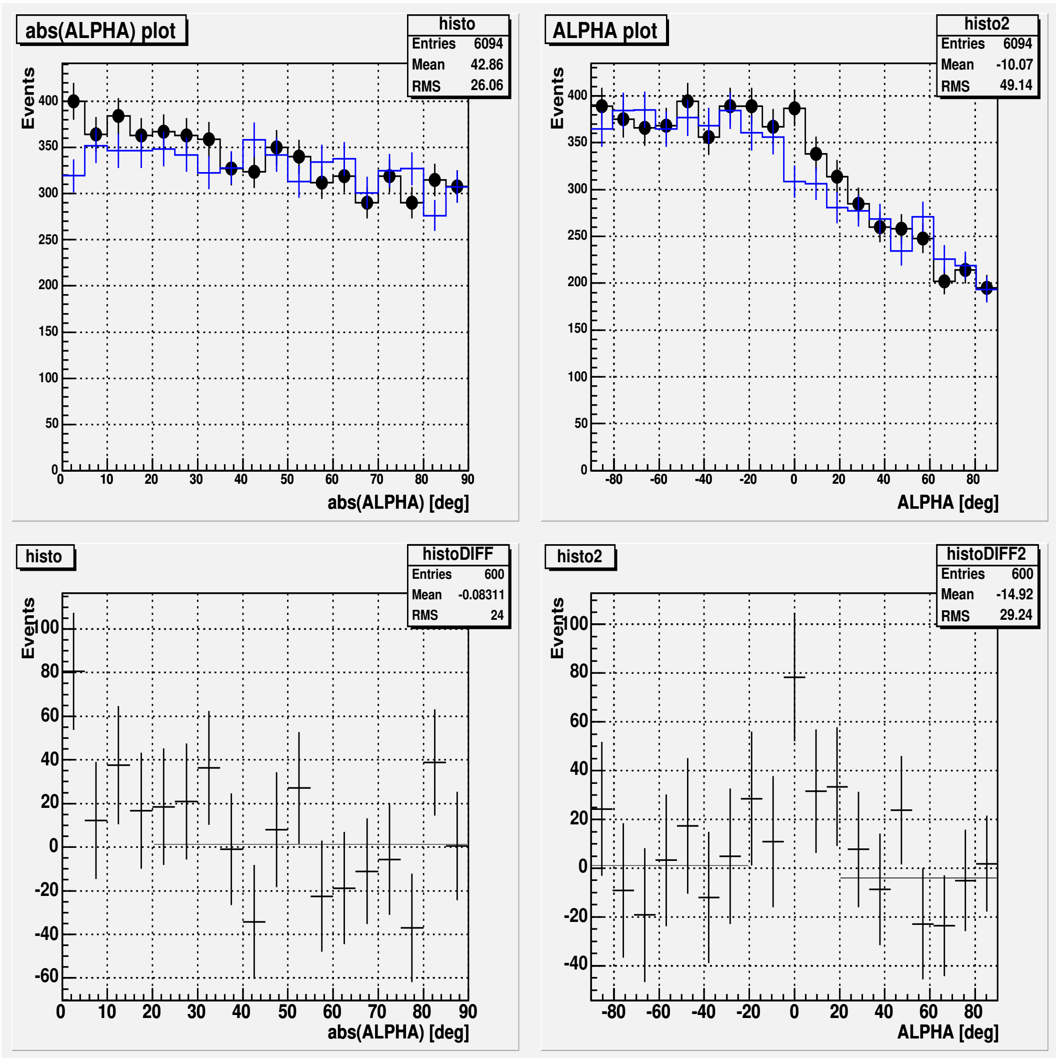

Figure 39: **HB-1553** ($\sigma = 2.75$ [LiMa 15deg]) optimize using MC gamma. Common cuts & SIZE>300 phe & HADR.<0.025.

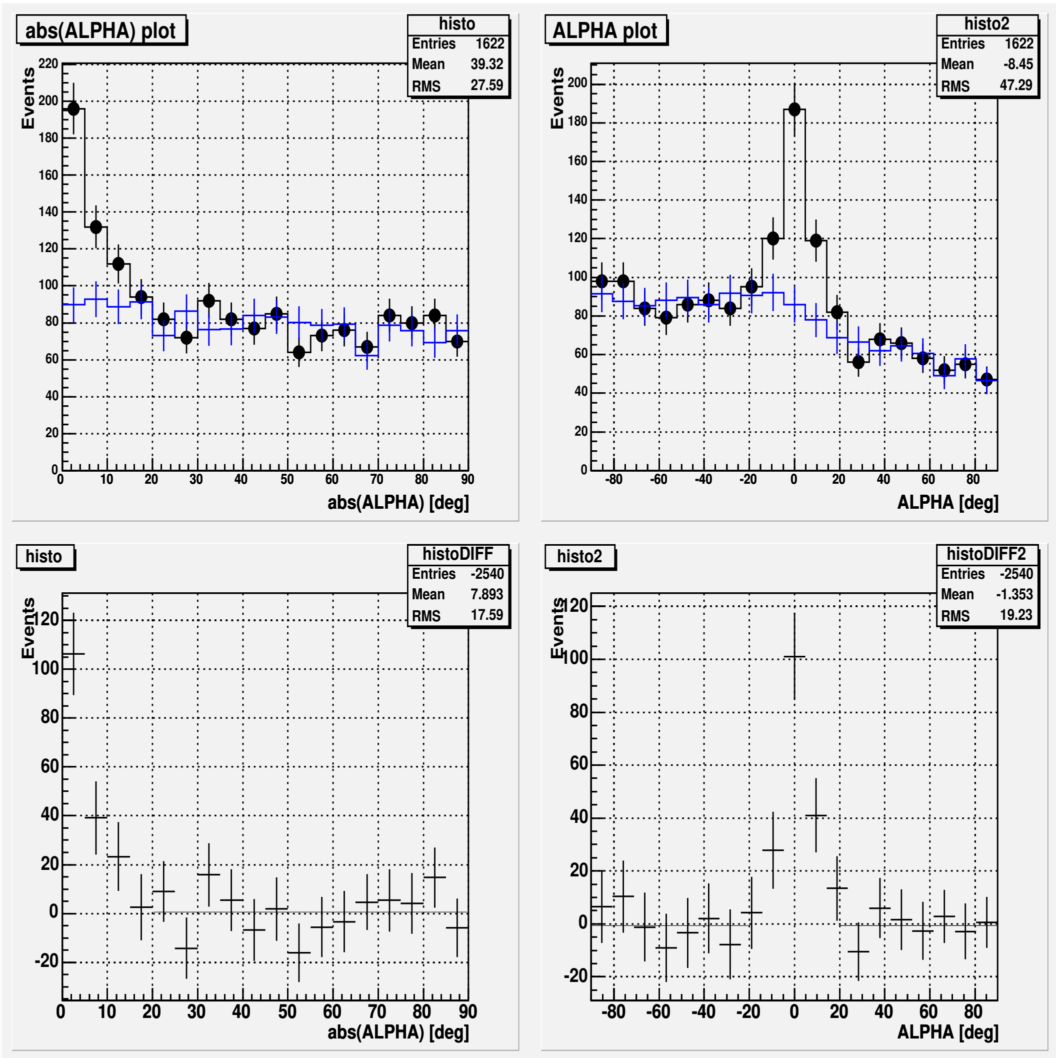

Figure 40: **Mrk501** (σ = 7.91 [LiMa 15deg]) optimize using MC gamma. Common cuts & SIZE>300 phe & HADR.<0.015.

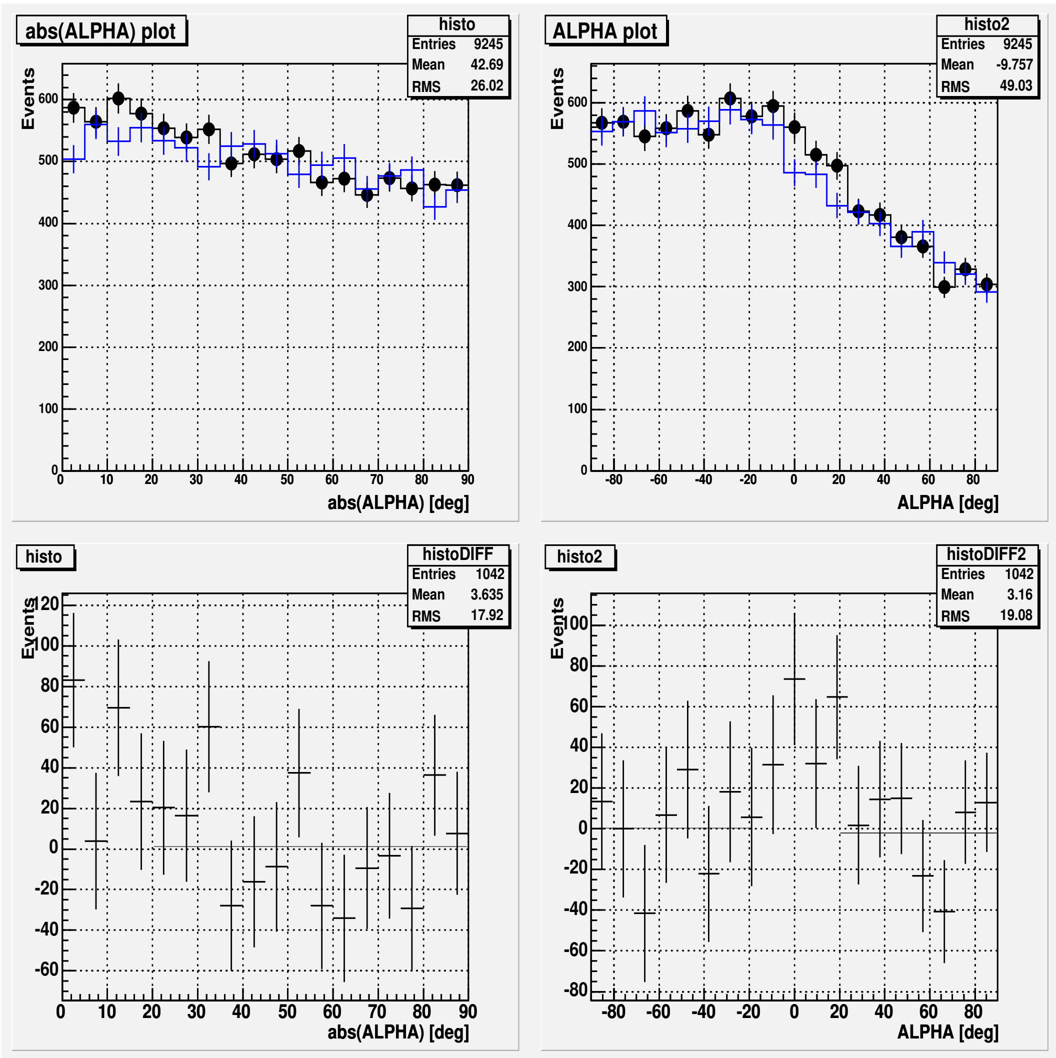

Figure 41: **HB-1553** (σ = 0.05 [LiMa 15deg]) optimize using Mrk501. Common cuts & SIZE>300 phe & HADR.<0.01.

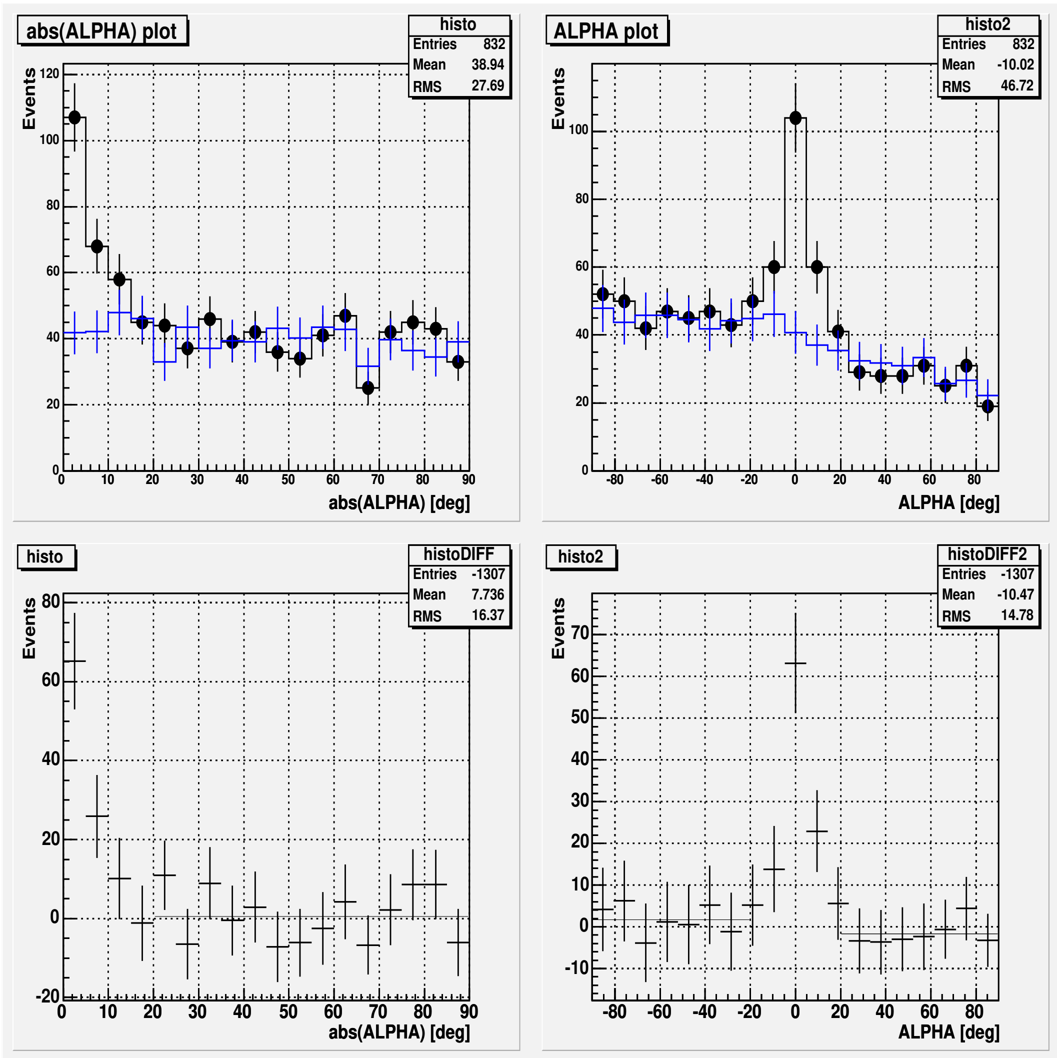

Figure 42: **Mrk501** ($\sigma = 6.68$ [LiMa 15deg]) optimize using Mrk501. Common cuts & SIZE>300 phe & HADR.<0.005.

A.3 100 phe < SIZE < 500 phe bin

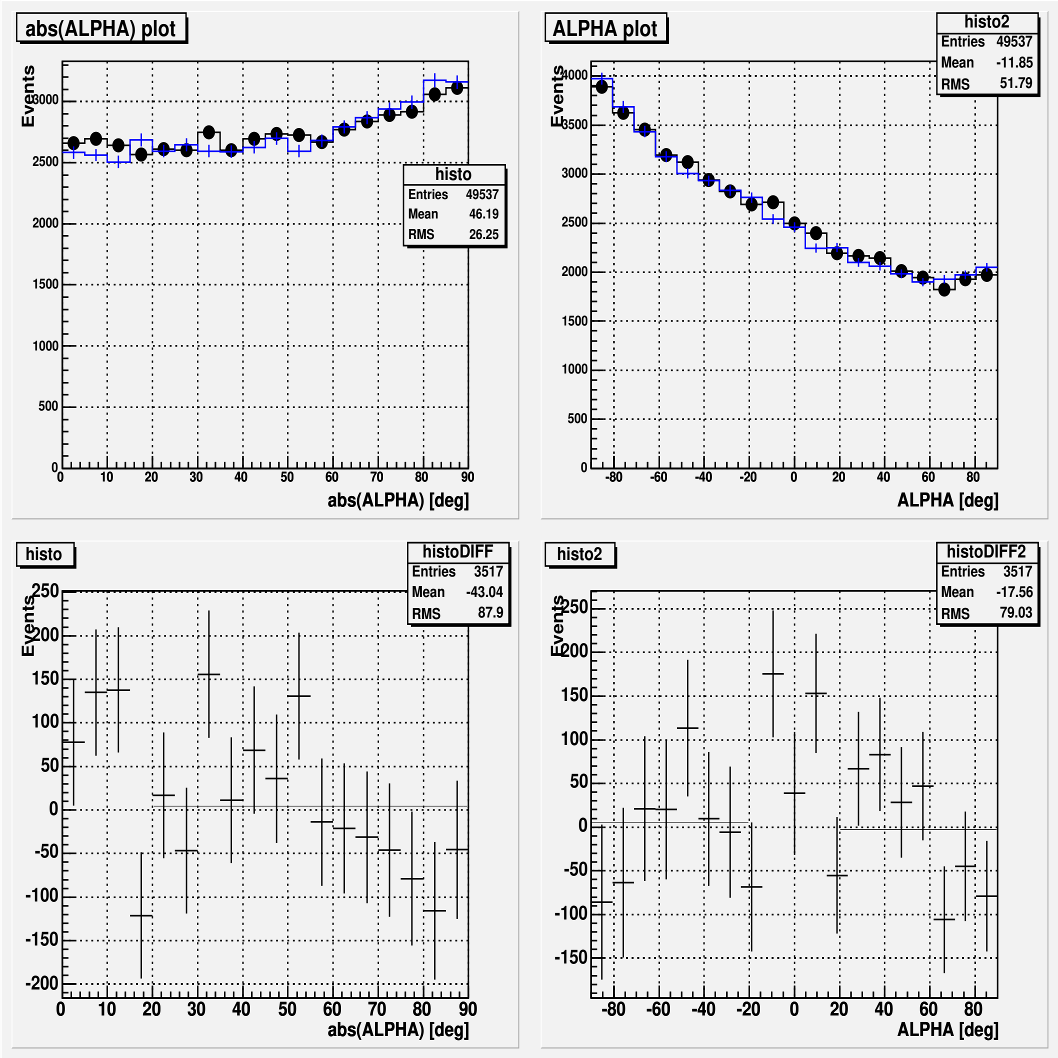

Figure 43: **HB-1553** (σ = 2.75 [LiMa 15deg]) optimize using MC gamma. Common cuts & 100 phe<SIZE<500 phe & HADR.<0.105.

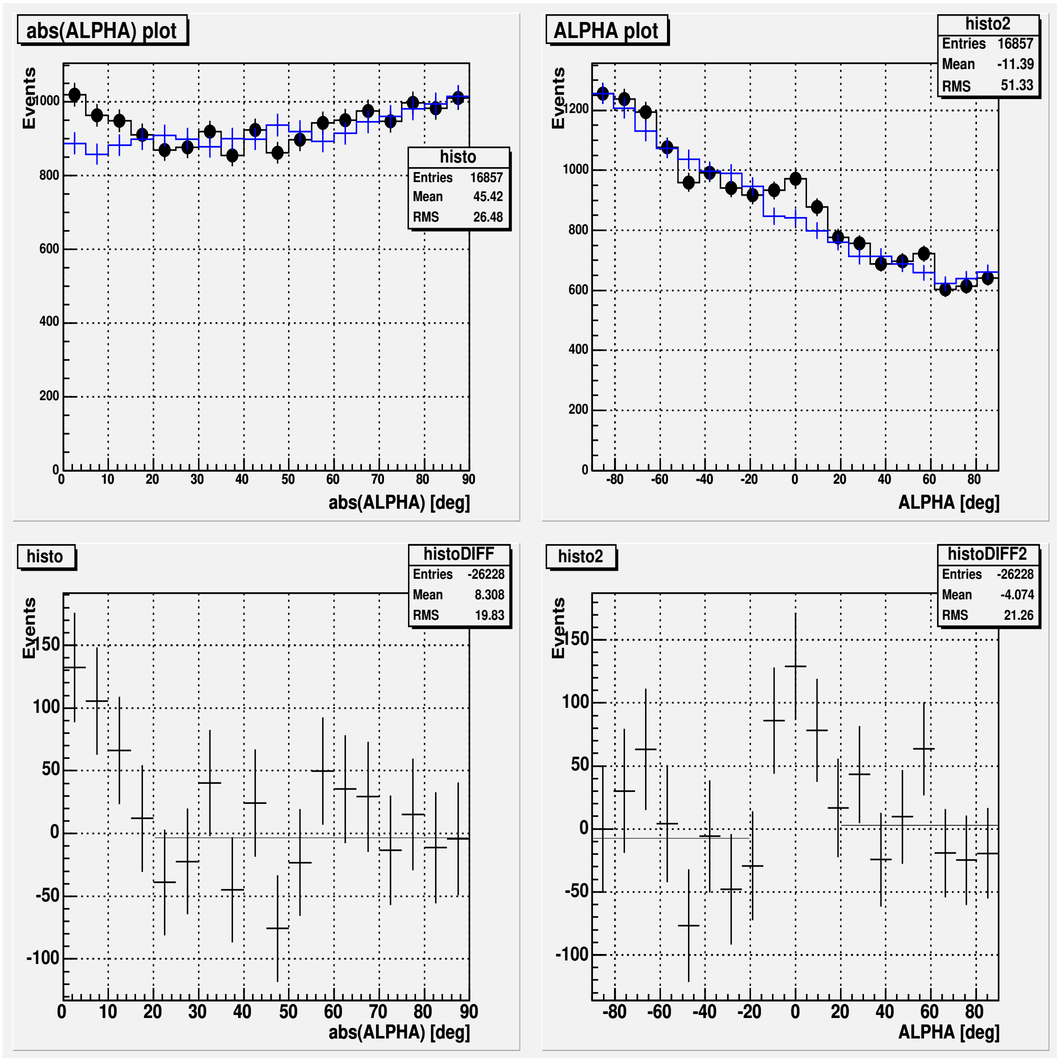

Figure 44: **Mrk501** (σ = 4.92 [LiMa 15deg]) optimize using MC gamma. Common cuts & 100 phe<SIZE<500 phe & HADR.<0.085.

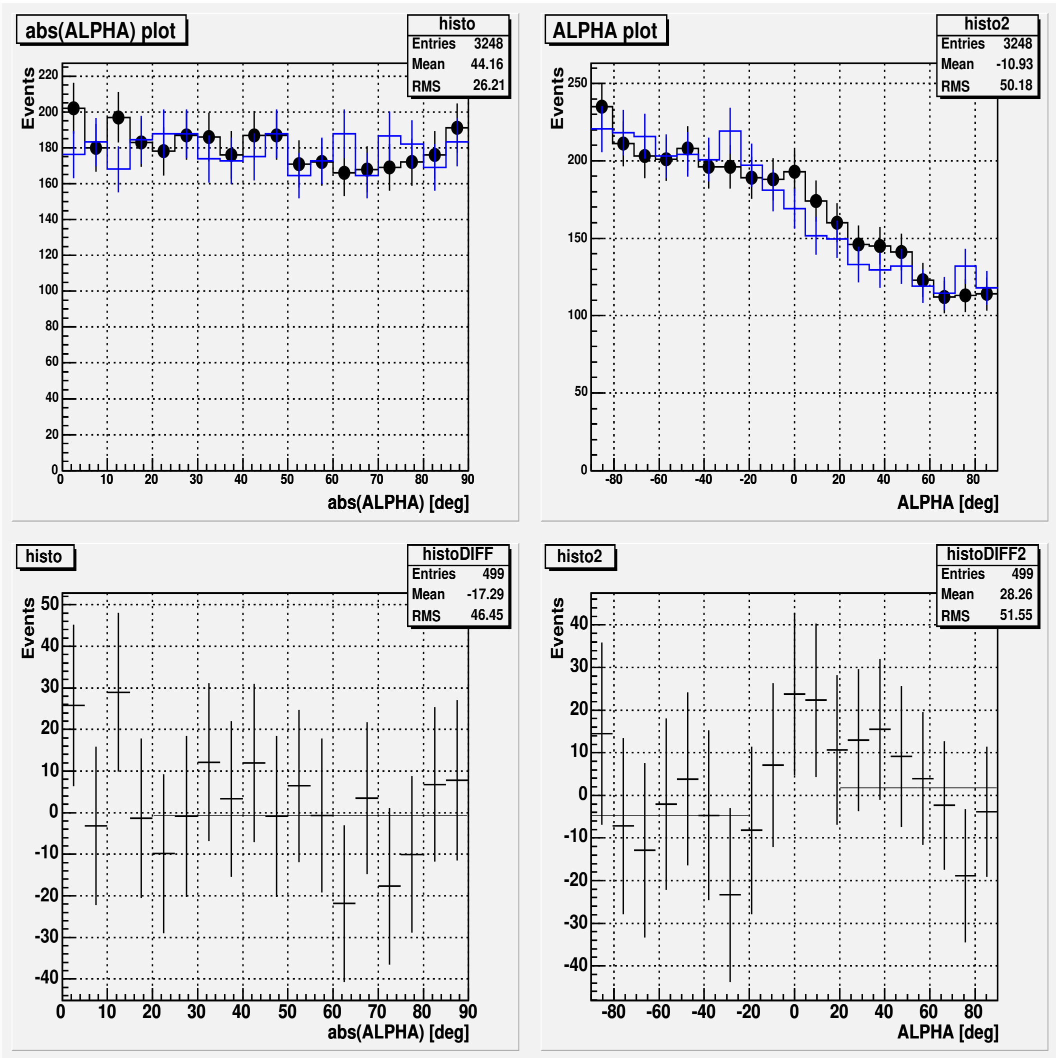

Figure 45: **HB-1553** (σ = 1.49 [LiMa 15deg]) optimize using Mrk501. Common cuts & 100 phe<SIZE<500 phe & HADR.<0.02.

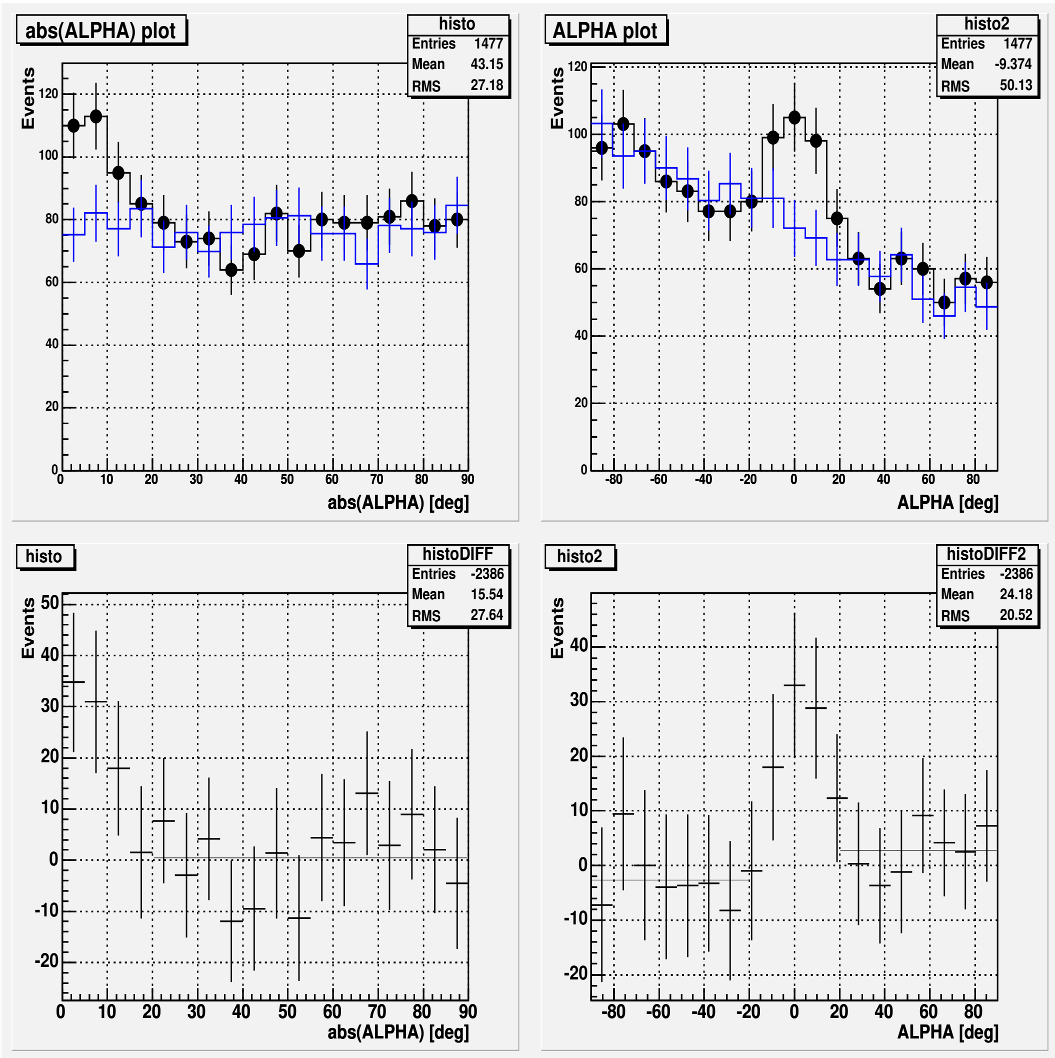

Figure 46: **Mrk501** ($\sigma = 4.38$ [LiMa 15deg]) optimize using Mrk501. Common cuts & 100 phe<SIZE<500 phe & HADR.<0.015.

References

[1] N.Carangelo et al., "Spettroscopy of BL Lac Objects: new redshifts and mis-identified sources", *astro-ph/0210016 v1*

[2] L.Costamente and G.Ghisellini, "TeV candidate BL Lac objects", *astro-ph/0112201*

[3] D.Dorner, talk: "Analysis of HB891553", *http://cds.mppmu.mpg.de/cdsagenda/fullAgenda.php?ida=a0541*

[4] *http://www.astro.uni-wuerzburg.de/results/pointing.html*

[5] P.Liebing, *http://wwwmagic.mppmu.mpg.de/documents/TDAS_notes/tdas0508/tdas0508.htm*

[6] W.Wittek, MAGIC-TDAS 02-03, *Image Parameters*

[7] Mars /mbasic/MMath.cc *ApJ 272 (1983) 317, Formula 17*

[8] E.Domingo Santamaria et al., "DISP analysis method for point-like off-axis and/or extended sources", Proceedings of 29th ICRC (2005) or *astro-ph/0508244*